HHS Public Access

Author manuscript

Biomaterials. Author manuscript; available in PMC 2024 November 05.

Published in final edited form as:

Biomaterials. 2023 October ; 301: 122260. doi:10.1016/j.biomaterials.2023.122260.

Next Generation 3D-Printed Intravaginal Ring for Prevention of HIV and Unintended Pregnancy

Isabella C. Young[1], **Priya Srinivasan**[2], **Roopali Shrivastava**[3], **Rima Janusziewicz**[3], **Allison Thorson**[3], **Mackenzie L. Cottrell**[4], **Rani S. Sellers**[5], **Craig Sykes**[4], **Amanda Schauer**[4], **Dawn Little**[6], **Kristen Kelley**[7], **Angela D. M. Kashuba**[3], **David Katz**[8], **Richard B. Pyles**[9], **J. Gerardo García-Lerma**[2], **Kathleen L. Vincent**[10], **James Smith**[2], **S. Rahima Benhabbour**[1,3,*]

[1]Division of Pharmacoengineering and Molecular Pharmaceutics, UNC Eshelman School of Pharmacy, University of North Carolina at Chapel Hill, Chapel Hill, NC, 27599, USA

[2]Centers for Disease Control and Prevention, Atlanta, 30333, USA.

[3]Joint Department of Biomedical Engineering, North Carolina State University and The University of North Carolina at Chapel Hill, Chapel Hill, NC, 27599, USA.

[4]Division of Pharmacotherapy and Experimental Therapeutics, UNC Eshelman School of Pharmacy, University of North Carolina at Chapel Hill, Chapel Hill, NC, 27599, USA

[5]Pathology Services Core, Lineberger Comprehensive Cancer Center, University of North Carolina School of Medicine; Chapel Hill, NC, USA

[6]Katmai Government Services, Anchorage, AK, 99515, USA

[7]The DESA Group, Columbia, SC 29223, USA

[8]Department of Biomedical Engineering, Duke University, Durham, NC, 27708, USA.

[9]Department of Pediatrics, University of Texas Medical Branch, Galveston, TX, 77555, USA.

[10]Department of Obstetrics and Gynecology, University of Texas Medical Branch, Galveston, TX, 77555, USA.

[*]Corresponding author: S. Rahima Benhabbour, benhabs@email.unc.edu.

Author Contributions

Conceptualization: SRB, JS, DK, KLV, RBP
Methodology: SRB, JS, KLV, RBP, ICY, PS, MLC, RSS
Investigation: ICY, RS, ALT, KLV, PS, MLC, CS, AS, RSS, RJ, JS, SRB
Visualization: ICY, RBP, PS, KLV, RJ, JS, SRB
Funding acquisition: SRB, DK, KLV, JS, RBP, JGGL, ADMK
Project administration: SRB, JS, KLV, RBP, DK, MLC
Supervision: SRB, JS, KLV, RBP, DK, MLC, ADMK, JGGL
Writing – original draft: ICY, PS, RBP, KLV, JS, RSS, AS, RJ, SRB
Writing – review & editing: ICY, SRB, PS, RBP, KLV, JS

Declaration of interests

The authors declare the following financial interests/personal relationships which may be considered as potential competing interests: S.R.B and R.J. are inventors on a patent issued by the US PTO 507074848 describing geometrically complex intravaginal rings and their methods of fabrication and are co-founders of AnelleO, Inc., which has licensed this patent. S.R.B and R.J. are also inventors on a PCT patent application (PCT/US21/50949) describing the post fabrication drug loading process.

Abstract

Globally, there are 20 million adolescent girls and young women living with HIV who have limited access to long-acting, effective, women-controlled preventative methods. Additionally, although there are many contraceptive methods available, globally, half of all pregnancies remain unintended. Here we report the first 3D printed multipurpose prevention technology (MPT) intravaginal ring (IVR) for HIV prevention and contraception. We utilized continuous liquid interface production (CLIP™) to fabricate MPT IVRs in a biocompatible silicone-based resin. Etonogestrel (ENG), ethinyl estradiol (EE), and islatravir (ISL) were loaded into the silicone poly(urethane) IVR in a controlled single step drug loading process driven by absorption. ENG/EE/ISL IVR promoted sustained release of drugs for 150 days in vitro and 14 days in sheep. There were no adverse MPT IVR-related findings of cervicovaginal toxicity or changes in vaginal biopsies or microbiome community profiles evaluated in sheep. Furthermore, ISL IVR in macaques promoted sustained release for 28 days with ISL-triphosphate levels above the established pharmacokinetic benchmark of 50–100 fmol/10^6 PBMCs. The ISL IVR was found to be safe and well tolerated in the macaques with no observed mucosal cytokine changes or alterations in peripheral CD4 T-cell populations. Collectively, the proposed MPT IVR has potential to expand preventative choices for young women and girls.

Graphical Abstract

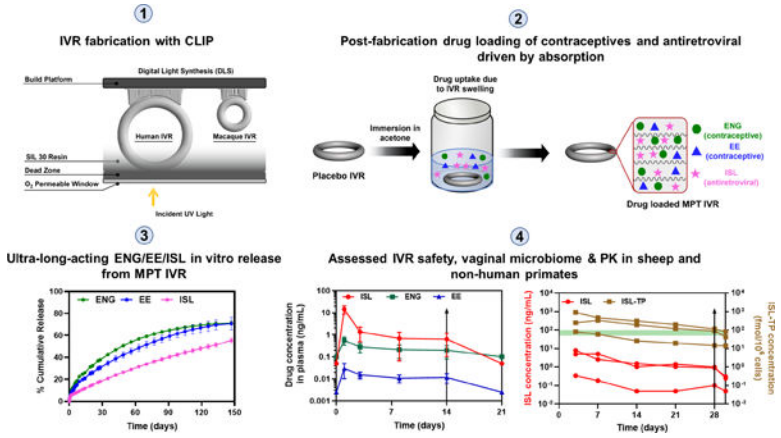

Keywords

contraception; drug delivery; HIV; intravaginal rings; 3D printing

Introduction

Globally, approximately 20 million adolescent girls and young women (AGYW) endure the burden of living with HIV and women and girls accounted for 63% of all new HIV infections in sub-Saharan Africa in 2020 [1]. Specifically, in sub-Saharan Africa, women are twice as likely to be infected with HIV than men and ~86% of new HIV infections are amongst adolescent girls (15–19 years old) [1]. Despite these striking statistics, until late 2021, only oral antiretroviral (ARV) therapies (tenofovir disoproxil fumarate (TDF) and

emtricitabine (FTC)) for HIV pre-exposure prophylaxis (PrEP) were available for women. However, some people find it difficult to adhere to daily oral regimens and, therefore, cannot fully benefit from PrEP. Fortunately, as of December 2021, cabotegravir long-acting injectable was approved for HIV PrEP for men and women [2, 3] which has potential to increase adherence due to reduced dosing frequencies. Additionally, in January 2021, the World Health Organization recommended the 30-day dapivirine intravaginal ring as an additional prevention choice for women to be used in combination with other prevention methods [4, 5]. Nevertheless, HIV PrEP for women continues to be extremely limited with the need for more long-acting, women-controlled, and highly effective options.

In addition to being disproportionately affected by HIV, women also disproportionately carry the responsibility for family planning. Nearly all contraceptive methods, except for male condoms and male sterilization, are female-based methods. Although 44% of women worldwide are on modern contraceptive methods (e.g. oral contraceptive pills, intrauterine device, injection, implant, vaginal ring), nearly half of all pregnancies remain unintended [6]. Despite the myriad contraceptive options available, condoms are the only product that protects against both HIV and unintended pregnancy. However, condoms elicit poor user adherence and require partner cooperation. Studies have shown that young women and girls are in favor of more technologies that serve multiple sexual or reproductive indications, particularly if they are discrete and long-acting [7–9]. Therefore, the development of multipurpose prevention technologies (MPTs) can fill the gap in the sexual and reproductive landscape by preventing multiple indications in an all-in-one technology [10].

We propose the development of a long-acting (≥ 90 days) MPT intravaginal ring (IVR) for the prevention of HIV and unintended pregnancy. IVRs are discrete, women-controlled, and a well-established delivery system that can promote long-acting release and are compatible with many active pharmaceutical ingredients (APIs) for a variety of indications (e.g., contraception, hormone replacement therapy, HIV prevention) [11–13]. Additionally, IVRs allow for significant drug uptake due to highly vascularized tissue in the vagina while bypassing first-pass metabolism [12]. There are many MPT IVRs in development and many IVR products in the market (e.g., NuvaRing®, Annovera®, Estring®) [10, 13]. Despite this, nearly all IVRs in development or currently available are manufactured with hot-melt extrusion and injection molding. With this traditional IVR manufacturing method, the polymer and API(s) are heated, mixed, and extruded into a mold to produce the final product for simple drug-loaded matrix rings or materials are co-extruded to form rods, cut to a desired length and then thermally welded into the final ring shape which is typically seen with reservoirs style or segmented IVRs [14]. Although this process is extremely high throughput and successful, this process exposes the material and APIs to high heat and pressure, which may limit material and APIs choices, particularly those that may be sensitive to these conditions. Additionally, injection molding has a negligible design space for IVRs resulting in a solid cross section which can promote incomplete drug release and requiring manufacturers to overload the device with APIs to achieve therapeutic efficacy [15]. Eliminating the solid cross-section and incorporating design can promote complete drug release and provide more opportunities to fine-tune drug release.

Additive manufacturing or 3D-printing is compatible with computer aided design (CAD) which opens the opportunity to easily incorporate design within IVRs in ways that is not possible with traditional IVR manufacturing. Uniquely implemented IVR design brings possibilities to eliminate the solid cross-section and alter ring surface area and drug diffusion distances to fine-tune drug release and promote complete API release [16, 17]. Few attempts have utilized 3D printing for vaginal delivery systems, such as IVRs and pessaries, specifically utilizing fused deposition modeling or droplet deposition modeling [18–23]. These techniques consist of a layer-by-layer depositing of melted filament of polymer and drug over a build platform. Notably, the studies using these techniques showed the ability to generate unique design structures within the IVRs to fine-tune drug release rates and promote near complete drug release. However, additive manufacturing with fused deposition or droplet deposition modeling typically involves hot-melt extrusion methods, which may not be amenable to highly sensitive drugs. Additionally, these techniques involve layer-by-layer manufacturing which could potentially cause rigid and non-monolithic parts, which may not be comfortable for a device intended to be inside the body. Thus, we propose to utilize continuous liquid interface production (CLIP™) or digital light synthesis (DLS™) to fabricate IVRs in a biocompatible silicone-based resin (SIL30, Carbon Inc) in a fast, translational, and layerless process [16, 24]. Uniquely, CLIP incorporates oxygen into the fabrication process which inhibits resin polymerization or solidification. Thus, in oxygen dominated areas, such as near the oxygen permeable window where oxygen is fed, a region of uncured resin is generated, called the ‘dead zone’, which prevents the part from attaching to the window and allowing continuous and layerless production [24]. Ultimately, this results in high resolution parts that are smooth and monolithic [24, 25].

Here, we fabricated solid silicone-based MPT IVRs with CLIP to gain understanding on material and drug interactions and to serve as a model for release kinetics which will aid with efficient optimization when generating geometrically complex IVRs in the future. After fabrication, we utilized a novel post-loading method as previously described to accurately incorporate drug into our IVRs [17]. Briefly, IVRs uptake APIs when placed in a drug concentrated organic solution due to the swelling properties of the silicone poly(urethane) matrix (SIL30) which promote uniform and controlled API absorption. MPT IVRs included two hormonal contraceptives used in NuvaRing, etonogestrel (ENG) and ethinyl estradiol (EE), and the highly potent ARV, islatravir (ISL). ISL is the first in its class nucleoside reverse transcriptase translocation inhibitor (NRTTI) that is intracellularly phosphorylated to ISL-triphosphate (TP) to inhibit HIV replication [26]. ISL’s long-acting property and potency is attributed to its unique functional groups (4’-ethynyl, 3’-hydroxyl, and 2-fluoro) contributing to its long intracellular half-life (120 hours) and an EC_{50} (effective concentration) of 0.05–0.1 nM [26]. ISL is currently in development for HIV treatment and prevention as a once- daily, and weekly oral tablet and a once-yearly implant [27–31].

With this clinically translational drug regimen, we assessed in vitro release, stability, vaginal microbiome, and performed pharmacokinetic (PK), and safety studies in sheep with the ENG/EE/ISL MPT IVR. Sheep were used as a human model due to their anatomical similarities, such as similar size vaginal canal and body mass [32] and thus allowed us to use human-sized IVRs for sheep PK and safety studies. We also assessed PK and safety of

ISL IVRs in macaques which is a highly relevant animal model for HIV therapies and PrEP. Collectively, we demonstrated the ability to develop a 3D-printed MPT IVR in a unique and biocompatible silicone-based material, incorporated three APIs using a novel single-step post-fabrication loading method, and showed sustained release of all APIs in vitro and in vivo with no evidence of toxicity in either animal model. MPT IVRs also had no negative impacts when tested in ex vivo human vaginal mucosal cultures colonized by eubiotic or dysbiotic microbiome communities.

Results

IVR fabrication with continuous liquid interface production (CLIP™)

Human-sized solid IVRs (used for sheep studies due to anatomical similarities) and macaque-sized solid IVRs were created using CAD and fabricated with CLIP 3D printing with a two-part silicone poly(urethane) (SIL30, Carbon Inc) resin. Notably, input parameters within the Carbon algorithm were unchanged when printing the differently sized IVRs (Fig. 1A). During fabrication, the dual resin selectively solidifies upon exposure to ultraviolet (UV) light via free radical polymerization to generate the solid IVR designed in CAD [16, 17, 24] (Fig. 1A). Oxygen was fed into the system through an oxygen permeable window to inhibit polymerization [16, 17, 24, 25]. This resulted in a region of uncured resin in an oxygen dominated layer, referred to as the ‘dead zone’ [16, 17, 24, 25], which allowed for continuous and layerless fabrication of the IVR. After the UV cure, IVRs underwent an 8 hour thermal post cure to initiate a secondary reaction and complete the matrix formation and produce the final IVR [16] (Fig. 1A). IVRs were smooth and monolithic due to the continuous fabrication process with mechanical properties as previously described [16]. Fig. 1B and C show human- and macaque-sized IVRs with their respective mass and dimensions.

Post-fabrication drug loading and loading equations

APIs were incorporated into the IVR post-fabrication and post-thermal cure via a solvent-mediated post-loading process [17] avoiding exposure to heat during the fabrication process. Separating ring fabrication and drug incorporation avoids exposure to harsh conditions, such as heat and UV light. Although the APIs used in this study can withstand these conditions and have high thermal degradation temperatures (>120°C), this technique can also be applied to more sensitive drugs in the future. Additionally, drug loading post-fabrication allows APIs to be accurately and homogenously dispersed throughout the matrix, which may not be achieved if APIs were incorporated in the resin during ring fabrication as subsequent washing steps may decrease total drug amount. Figure 1D depicts a schematic of the IVR drug loading process with ENG/EE/ISL. Due to the unique material properties the SIL30, IVRs swell considerably when placed in a drug containing acetone solution, referred to as the loading solution. The swelling process is driven by hydrophobic interactions between the material and the solvent, which allows for API(s) absorption and homogenous distribution within the IVR matrix [17] (Fig 1D). Acetone was selected as the solvent for drug loading since it considerably swells the silicone-based IVR matrix, elicits high drug solubility with ENG, EE, and ISL, has a low flashpoint, and is classified as a safe solvent (Class 3) [33]. We developed a weight-based loading approach to achieve target drug loading in our IVRs, referred to as loading equations. Loading equations elicit a linear relationship between drug

weight percent ((mass of drug loaded/mass of IVR) × 100) and the concentration of the loading solution. Loading equations for ENG, EE, and ISL are shown in Figure 1E–H. Human-sized IVRs (54 mm outer diameter (OD), 7.6 mm cross-sectional diameter (CSD)) used for in vitro release studies and sheep studies were loaded in a single step process with three APIs of different physiochemical properties. Each IVR contained approximately 14 mg ENG, 3 mg EE, and 300 mg ISL utilizing the APIs respective loading equation. In vitro release studies and non-human primate studies with macaque-sized IVRs (25 mm OD, 6.0 mm CSD) were loaded with 62 mg ISL, which was a similar ISL weight % loading to human-sized IVRs (3.3 weight % for macaque-sized IVRs and 3.9 weight % for human-sized IVRs).

In vitro drug release of MPT (ENG/EE/ISL) IVR

After drug incorporation into the IVR, an in vitro release study of the ENG/EE/ISL IVR, referred to as MPT IVR, was carried out with human-sized IVRs in simulated vaginal fluid (SVF) [34] at pH 7 to mimic the vaginal environment of the sheep model [35]. Here, we assessed feasibility of co-formulating three APIs in a single IVR (MPT IVR), investigated if the MPT IVR elicited long-acting release (≥ 90 days), and determined presence of potential drug-drug interactions by comparing in vitro release profiles from the MPT IVR (ISL/ENG/EE) and an ISL only IVR and an ENG/EE IVR. Results showed that in vitro release was sustained for 150 days and elicited a low burst in the first 24 hours for all drugs (< 7% burst release) (Fig. 2A). Notably, the hydrophilic drug ISL exhibited zero-order release kinetics for the entire duration of the in vitro release study, whereas the hydrophobic hormones ENG and EE demonstrated root time kinetics after a burst release. Additionally, we assessed in vitro drug-drug interactions by investigating the in vitro release profile of ISL alone (Fig. 2B) and the hormones alone (Fig. 2C) compared to when formulated as an MPT. Daily release profiles are demonstrated in Fig 2D–F for all drugs when formulated as an MPT or as a single indication. In vitro release of ISL alone and ENG/EE were comparable ($p>0.05$) to API release when formulated together as an MPT demonstrating absence of in vitro drug-drug interactions in the MPT IVR. After 150 days of in vitro release from the MPT IVR, ISL released 55.40±2.70%, ENG released 71.19±1.76%, and EE released 70.72±5.65% of the total payload. After in vitro release studies, IVRs were dried and had approximately a 3% increase in outer diameter, 5% increase in cross-sectional diameter, and a 7% increase in mass compared to the beginning of the study.

Post-storage in vitro release kinetics of MPT IVR

To determine the stability of the MPT IVR during storage, we performed a 90-day storage study under accelerated storage conditions at 40°C/75% relative humidity (RH). An increase in IVR mass (2.5% increase) and outer diameter (1.1% increase) was observed post storage, which is likely attributed to water intake and slight IVR swelling due to humidity exposure during storage (Fig. S1). Additionally, IVRs exhibited <10% change in drug content post storage; however, all APIs remained stable with no change in peak shape or retention time from the HPLC analysis (Fig. S1). A post-storage in vitro release study was carried out to compare release kinetics against baseline (t=0) as shown in Fig. S2A.

ENG and EE release after storage was comparable ($p > 0.05$) to baseline up to 90 days (Fig. S2B, D, and E), whereas ISL elicited approximately a 3-fold increase in burst release compared to baseline (44304±2070 μg ISL released after storage compared to 14633±919 μg released ISL at baseline after 24 hours) (Fig. S2C and S2F). This significant increase ($p<0.05$) can potentially be attributed to changes in the IVR matrix, notably its minimal swelling due to water intake after storage resulting in higher initial release of the hydrophilic ARV. Nevertheless, ISL release before and after storage became similar after approximately one month ($p>0.05$) (Fig. S2C).

Sheep pharmacokinetics of MPT IVR

A 21-day in vivo pharmacokinetic (PK) study was carried out with the human-sized MPT IVR in 4 female sheep. The study design for the sheep PK study is shown in Figure 3A where plasma, vaginal tissue, vaginal fluids, and rectal fluids were collected throughout the study. MPT IVRs were removed after 14 days, and plasma and fluids were collected 7 days post IVR removal to assess the presence of a PK tail. Both vaginal and rectal tissue concentrations were measured as both genital tissues are primary routes of sexual transmission of HIV. Figure 3B–F represent the in vivo concentrations of ISL, ENG, and EE in plasma, vaginal tissue, and fluids. Drug levels were maintained during the 14-day period for all APIs in all compartments. After 7 days post IVR removal, almost all plasma and fluid samples were below the limit of quantification demonstrating a short PK tail for all APIs. IVRs retrieved after the in vivo study and exhibited approximately a 7% increase in mass, a 2% increase in outer diameter, and 1% increase in cross-sectional diameter. Retrieved IVRs were extracted to quantify residual drug and results showed that 72.14±3.62% of ISL, 63.43±1.89% of ENG remaining, and 76.68±3.69% of EE were remaining in the MPT IVR at the end of the pilot PK study.

Sheep safety studies with MPT IVR

Local tolerability was assessed in 4 age and breed-matched sexually mature sheep (Fig. 4 and Fig S6). Two untreated control animals were also age and breed-matched to the treated animals (Fig. S6 and S7). Vaginal biopsies from treated sheep were collected at Day 0, 8, and 14 after vaginal insertion of the MPT IVR. Comparator controls were collected at Day 1, 8, and 15.

There was no adverse MPT IVR related findings in the vaginal biopsies evaluated. MPT IVR related findings at Day 8 and/or 14 included an increased incidence and/or severity of epithelial hyperplasia, intraepithelial eosinophils, parakeratosis, and submucosal neutrophil and eosinophil infiltrates as compared to control animals (Fig. 4 and Fig. S7). Vaginal epithelial hyperplasia was not present in any MPT IVR treated sheep (n=4) at Day 0 but was present in all 4 sheep at Days 8 and 14 (3 minimal, 1 mild). No increases in the incidence or severity of epithelial hyperplasia were identified in the control sheep compared to Day 1 at Days 8 and 15. Similarly, the incidence and severity of parakeratosis was higher (maximum severity was mild) in MPT IVR treated sheep at Days 8 and 14 as compared to Day 0. The severity of parakeratosis was higher in MPT IVR treated sheep compared to control sheep at Days 8 and 15. Minimal superficial submucosal and mucosal eosinophil infiltrates were present only in MPT IVR administered sheep only at Day 8 and/or Day 14. Minimal to mild

neutrophil infiltrates were evident in the superficial submucosa of MPT IVR treated sheep, particularly in association with the superficial small vessels only at Day 8 and/or 14. Similar findings were not present in the control sheep.

Toxicity was also evaluated with colposcopy and optical coherence tomography (OCT). Colposcopy images were graded as previously described [36] with observations related to color change and intact or disrupted epithelium and blood vessels. OCT has been previously described [37], however, briefly, it is similar to ultrasound, but uses light rather than sound waves to interrogate tissue and determine tissue properties including the thickness of the epithelial layer. A single vaginal biopsy was taken at the lateral mid-vagina (days 0, 8, and 14), sectioned, stained with hematoxylin and eosin (H&E), and measured for epithelial thickness at 9 locations across the biopsy. There were no signs of toxicity by colposcopy or by vaginal epithelial thickness as measured by OCT or biopsy. At baseline on colposcopy, petechiae were noted in one MPT IVR treated sheep and during treatment, normal findings of erythema and/or petechiae were found in all sheep that used the MPT IVR (Table S4). There was no evidence of epithelial disruption, bleeding, or ulceration in any sheep. OCT imaging showed consistent thickness of the epithelial layer during the first 8 days of treatment, with no epithelial thinning (Figure 5A). Similarly, epithelial thickness from vaginal biopsies was consistent throughout the study in sheep treated with the MPT IVR, with no evidence of thinning of the epithelium (Figure 5B) associated with the treatment. These results are consistent with the epithelial thickness of naturally cycling sheep (60–90 μm) previously reported in the literature [37].

The community of vaginal microbiota and shed epithelia from the 4 sheep that wore the MPT IVR were analyzed at selected time points during the 14-day exposure and then on day 21 (Figure 5C and D), 7 days after the MPT IVRs were removed. DNA was extracted from vaginal wall swabs at baseline just prior to ring insertion (day 0) and then on days 1, 3, 8 and 14 while the MPT IVRs were in place and then on study day 21 (7 days after MPT IVR removal). Using a customized qPCR array for sheep vaginal microbiota targets [38] the total bacterial 16S rDNA level (each bacteria species encodes a variable copy number) and the number of sheep GAPDH (single copy gene) copies were quantified. Unexpectedly, 24 hours after MPT IVR placement, an average 10-fold increase in GAPDH copies was observed in vaginal swabs (Figure 5C red line; $p<0.05$ student's T test) in contrast to the consistent mucosal thickness observed by OCT. The elevated levels were maintained in all 4 sheep on day 3 and in 3 of 4 sheep on day 8 (Fig. S8). On day 14 when the MPT IVRs were removed, the average GAPDH level had returned to baseline based in 2 sheep with baseline or lower levels and 2 with still elevated sheep DNA (Fig. S8). On day 21, 7 days after MPT IVR removal, all 4 sheep showed baseline or lower levels of GAPDH. Placement of the MPT IVR was also associated with a significant increase in total 16S rDNA copies indicating an increase in vaginal microbiota collected in each vaginal swab (Figure 5C blue line; $p<0.01$ student's T test). The ~1000-fold increase in 16S rDNA copies was maintained while the MPT IVRs were in place and then dropped to near baseline levels in all 4 sheep on day 21 (Fig. S8). The potential impact on the vaginal community composition was evaluated by quantification of selected bacterial targets associated with both eubiosis and dysbiosis as previously reported [38]. The average community profile by sample day for the 4 sheep is shown as proportional bar charts (Figure 5D) that illustrate the observed

shift from an *Alloiococcus*/*Corynebacterium*-dominated community (day 0) to communities that were dominated by *E. coli*, an organism associated with non-inflamed, eubiotic vaginal samples [38, 39]. This finding was consistent for all 4 sheep. On day 21, after the MPT IVR was removed, the average community profile was still dominated by *E. coli* but had increased proportions of both *Alloiococcus* and *Corynebacterium*.

We also evaluated the sheep GAPDH and total 16S rDNA copy number associated with the fluid on the removed MPT IVR (Figure 5E, sample 0) and on 3 wedges (samples 1–3) collected from equidistant points on the used MPT IVRs. The average amount of sheep GAPDH and bacterial 16S was remarkably high and consistent across the fluid and wedge samples for all 4 MPT IVRs (Figure 5E) suggesting the MPT IVRs supported epithelialization followed by vaginal microbiota colonization based on the observed swab kinetics (Figure 5C). To confirm the MPT IVRs were not contaminated with *E. coli* prior to insertion, two unused rings were evaluated and found to contain <100 16S rDNA copies per wedge consistent with the level of bacterial DNA contamination found in PCR chemistries. Plating of culture medium from MPT IVRs soaked for 24 hours did not yield any colonies on Luria Bertani agar plates. Using the ovine vaginal microbiota qPCR array [38, 39] we evaluated the composition of the bacterial communities associated with the MPT IVR fluid and wedges finding a subset of the detected bacteria from the sheep, again dominated by *E. coli* (Figure 5F), leading us to hypothesize that the MPT IVR is epithelialized over the first 24 hours after placement followed by colonization with a reduced set of vaginal microbes present in the sheep vaginal vault.

Human vaginal microbiota studies with MPT IVR

To test the hypothesis that the MPT IVRs were epithelialized and colonized by vaginal microbes and to determine if the MPT IVR was detrimental to human vaginal environments, we tested mini MPT IVRs (3 mm OD and 1.0 CSD) printed to fit into a 24 well transwell insert in our human vaginal epithelial cell (VEC) culture model [40, 41]. The apical surface of the ALI VEC culture models the human vaginal lumen and supports colonization by transplanted vaginal microbiota [41, 42]. We have previously used this model system to study vaginal applicants and the impact of vaginal bacterial isolates and communities [41–43]. A pilot study was performed in matured ALI VEC cultures using placebo or MPT IVRs that were placed in 2 wells and incubated for 48 hours. Both standard photography (Figure 6A, left panel) and phase microscopy (4X magnification; right panels) illustrated that the IVRs were tolerated without obvious impacts to the multilayer.

In a second study, mature ALI VEC (6/condition) were either maintained sterilely (no vaginal microbiota; No VMB) or colonized for 24 hours with representative vaginal communities dominated by *Lactobacillus crispatus* (LC), *L. iners* (LI) or a diverse community from a donor with clinical bacterial vaginosis (BV). Mini MPT IVRs were placed and cultured for 48 hours and then sterilely removed. In VEC cultures with No VMB, neither the placebo nor MPT IVRs had significant impacts on transepithelial electrical resistance (TEER) values (Figure 6B; multiple t test with Mann-Whitney corrections) however, there was a trend of increased resistance. VEC colonized with either the LC- or LI-dominated communities and exposed to the placebo IVR confirmed no ring-based

impacts on TEER (no IVR versus placebo). Colonization with the BV community led to significant reductions in TEER in the absence of an IVR consistent with the expected damage caused by this dysbiotic group of bacteria. Interestingly, the MPT IVR led to significant increases in TEER values for each community (LC p=0.0009; BV p=0.00004; LI p=0.0007) relative to the equivalent no ring average (Figure 6B). DNA extracted from each culture was subsequently analyzed. The presence of the IVRs had minimal effect on the average community profile in the transwell cultures colonized by each community based on relative abundance of the organisms detected by the qPCR array (Figure 6C). Although some apparent shifts occurred none were found to be significant when absolute abundances were compared (data not shown).

Results from the qPCR array indicated that ALI VEC cultured with the placebo or MPT IVRs had no detectable differences in the number of human cells (human GAPDH; Figure 6D) or bacterial 16S rDNA copies (Figure 6E) over the 48-hour exposure. This was consistent with the lack of changes in the sheep mucosa by colposcopy, OCT and histology (Figure 4 and 5A). Further, the human GAPDH levels were indistinguishable from average GAPDH (horizontal line) in cultures that did not receive IVRs (Figure 6D). An expected, higher 16S rDNA levels were observed in the BV samples consistent with the outcomes for these community types relative to LC- and LI-dominated communities. To address whether placebo and MPT IVRs were epithelialized and colonized by bacteria, we evaluated the human GAPDH and 16S rDNA levels associated with IVR wedges as described above for the sheep study. Over the 48-hour exposure, both the placebo and MPT IVRs appeared to become epithelialized and colonized with substantial levels of GAPDH and 16S (Figure 6D and E, grey bars).

Although compelling and consistent, the DNA findings in sheep and human VEC cultures did not conclusively show that the IVRs were epithelialized and colonized, thus we evaluated the apical surface of IVRs that was not in direct contact with the top of the modeled mucosa. Initially, using scanning electron microscopy (SEM) (Figure 6F), we established the appearance of the surface of unused IVRs dry (top, 100X) or after 24h soaking in culture medium (bottom, 5000X). The uniform surfaces of unused IVRs showed expected outcomes of 3D printing including some grooves and depressions that were consistently visualized (Figure 6G, 5000X). The surface of IVRs incubated with VEC for 48 hours developed organic structures consistent with previously reported VEC mucosal surfaces that developed on the porous transwell membranes (34–36; Fig. 6H and 6I). The observed blebs were consistent with hypothesized glycogen and other extracellular vesicles (34, 35). As expected, these surfaces supported colonization by vaginal microbiota within 48 hours in cultures pre-colonized with the LC-dominated (Fig. 6J), LI-dominated (Fig. 6K) or BV (Fig. 6L–N) communities. The micrographs illustrate expected bacterial morphotypes at levels that were consistent with the quantified 16S rDNA (Fig. 6E).

ISL IVR in vitro release and in vivo pharmacokinetics in female macaques

Given that ISL has not been previously delivered topically and to assess clinical relevance of ISL release from our IVRs, we administered ISL only IVRs to female pig-tailed macaques and investigated drug concentrations in multiple matrices. Prior to macaque studies, we first

sought to assess the in vitro release of ISL in macaque-sized IVRs in SVF pH 8 to mimic the macaque vaginal environment [44]. ISL was loaded in macaque-sized IVRs at a similar weight % loaded in the human-sized MPT IVR. Fig. S9 demonstrates the sustained in vitro release of ISL over 90 days, with a low burst release (<6%) and zero-order release kinetics. Subsequent to promising in vitro release results, a 30-day in vivo PK study was carried out with the ISL IVR in 3 female pig-tailed macaques. Fig. 7A represents the study design of the macaque PK study, where plasma, vaginal tissue, vaginal fluids, rectal fluids, and peripheral blood mononuclear cells (PBMCs) were collected through the 30-day study. PBMCs were collected to extract and quantify ISL's active metabolite, ISL-triphosphate (ISL-TP), which is intracellularly phosphorylated to inhibit HIV replication [26, 45]. ISL IVRs were removed after 28 days and plasma, fluids, tissue, and PBMCs were collected 2 days later to assess drug levels post IVR removal. Fig. 7B–F represents the ISL concentrations in the various matrices. Throughout all compartments, ISL levels were maintained for 28 days and ISL-TP levels were at or above the established PK benchmark for oral dosing of 50–100 fmol/10^6 PBMCs [46]. In vaginal and rectal fluids (Fig. 7D–F) ISL levels dropped about a log from day 3 to 7 but remained stable until IVR removal at day 28, typical of matrix IVRs. At 2 days post-IVR removal, there was a 2–4-fold and 1.04–2.2-fold decrease in ISL in plasma and ISL-TP in PBMCs, respectively. Additionally, there was a 59.7–143.8-fold ISL decrease in proximal vaginal fluids, a 13.4–34.4-fold ISL decrease in distal vaginal fluids, and a 4.6–10.8-fold ISL decrease in rectal fluids 2 days post IVR removal. Quantification of residual drug in IVRs ex vivo showed that 55.3±3.58% ISL was remaining in the IVR after 28 days in macaques.

Macaque safety study with ISL IVR

We evaluated the in vivo vaginal safety of the ISL IVRs in three pigtailed macaques by monitoring their vaginal pH, mucosal cytokine, and chemokine concentrations, and systemic CD4 and CD8 frequencies in PBMCs. The macaques maintained their vaginal pH within the typical normal range of 5 to 8.5 over the entire study (Fig S10). Though a 1 to 1.5 log increase in vaginal pH on days 7 and 21 is seen in two of the three macaques, it was within the range that has been reported in other studies [47–49]. These two macaques were found to undergo menses on day 14. Friedman test found no significant difference in the increase in the vaginal pH on these days in comparison to the other time points ($p=0.1826$). Mucosal inflammation due to the presence of the ISL IVR was monitored by measuring 20 cytokines and chemokines in vaginal fluid collected throughout the study (Fig. S11). Freidman test of the log transformed concentrations showed no statistically significant changes in any of the cytokine or chemokine levels due to the presence of the ISL IVR. As CD4+ T cells are the main targets required for HIV infection, and CCR5 serves as the primary coreceptor for HIV entry we chose to monitor both CD4, and CD4+CCR5+ populations longitudinally [50]. Like the CD4+ and CD4+ CCR5+ T cells, a routine evaluation of CD3, CD8, and CD4 memory subtypes (CD4+T_{CM}-central memory, CD4+ naïve, CD4+T_{EMRA}-terminally differentiated effector memory, and CD4+T_{EM}-effector memory) also revealed stable frequencies in PBMC obtained throughout the study (Fig 8). Kruskal-Wallis test of the T cell frequencies and the CD4 subsets did not show any statistically significant differences while the IVR was present in comparison to prior to ring insertion (day 0) and post IVR removal (day 30). The stable T cell frequencies after IVR administration is

significant as recent human data showed a reduced lymphocyte and CD4 cell count after oral administration of ISL [51, 52].

ISL phosphorylation capacity in sheep PBMCs and extrapolation of ISL-TP in sheep PK samples

As mentioned previously, ISL-TP is the therapeutically active metabolite of ISL to prevent HIV infection and thus, it is crucial to determine concentrations of ISL-TP to accurately interpret PK data and assess clinical relevance. However, levels of ISL-TP in PBMCs extracted from sheep plasma in the PK study were below the limit of quantification and as such could not be determined. This effect can potentially be explained if sheep elicit a low ISL phosphorylation capacity. A recent in vitro study found that the intracellular pharmacology of ISL differs between species, with humans and non-human primates eliciting the greatest phosphorylation capacity when compared to rats, dogs, minipigs, and rabbits [45]. We conducted a similar study to determine the phosphorylation capacity of ISL in sheep PBMCs in vitro. Results showed that sheep PBMCs have 111-fold lower ISL phosphorylation capacity compared to human PBMCs when dosed with 500 ng/mL ISL, which explains the inability to detect any ISL-TP in sheep PBMC samples from the PK study (Fig. 9A). ISL-TP levels were below the limit of quantification when sheep PBMCs were dosed with lower ISL concentrations (5 ng/mL and 50 ng/mL).

Although sheep have a low ISL phosphorylation capacity, a recent study suggested a strong correlation between ISL-TP in PBMCs and ISL plasma levels [53]. Thus, we determined a ratio of ISL-TP to ISL in plasma from the ISL IVR macaque PK data that can be used to extrapolate ISL-TP levels in the sheep PK study. We determined the median (range) of the ISL-TP to ISL in plasma ratio to be 174.9 (54–536). Applying this ratio to the observed ISL levels in sheep, ISL-TP levels were extrapolated as shown in Fig. 9B. These data show that the estimated ISL-TP levels were at the established PK benchmark of 50–100 fmol/10^6 PBMCs. However, it is important to note that the estimated ISL-TP levels do not represent expected levels in the sheep model since sheep have a much lower phosphorylation capacity compared to macaques, which is the basis of the calculated ratio used to extrapolate ISL-TP levels. Instead, these levels could potentially represent expected levels to be observed in humans given that sheep elicit similar size vaginal anatomy and body mass relative to humans [32], and human and macaques have similar ISL phosphorylation capacities [45].

Discussion

We report on a first-in-line 3D-printed MPT IVR utilizing a state-of-the-art CLIP 3D-printing technology, and a clinically translational drug regimen. We demonstrated long-acting release of ENG/EE/ISL in vitro and sustained drug concentrations of the APIs in sheep and macaques for 14 and 28 days, respectively, a time at which the rings were removed. There were no signs of toxicity in the sheep that wore the MPT IVR based on colposcopy, OCT, and vaginal biopsies as well as molecular analyses of sheep GAPDH, bacterial 16S and VMB community profiles. In fact, the VMB analyses suggested the presence of the MPT IVR increased the presence of bacteria associated with vaginal eubiosis in sheep (31, 32). Studies in a culture model of human vaginal mucosa supported the

findings in sheep and, through SEM, indicated that the MPT IVRs were epithelialized and colonized by a subset of vaginal bacteria. In macaques, the ISL IVR was found to be well tolerated and no safety issues were observed with mucosal cytokines, vaginal pH, or CD4 T cell frequencies in PBMC over the 28-day study period.

Using CLIP 3D printing, IVRs were fabricated with a fast, layerless, scalable, and translational manufacturing process and a biocompatible silicone-based material which resulted in monolithic and smooth IVRs. The hydrophobic silicone-urethane matrix considerably swells when placed in an organic solvent, such as acetone. Leveraging this material property, a drug loading process was developed and used to load APIs into the IVRs via absorption. Using drug loading equations developed and validated for each API, target amounts of ENG (Log P 3.32), EE (Log P 3.67), and ISL (LogP −1.19) were loaded into the IVR in a single step process to yield the ENG/EE/ISL MPT IVR. This IVR manufacturing process is, to our knowledge, the first to combine 3D-printing for ring fabrication and post-fabrication drug incorporation while allowing complete intercalation of one or multiple drugs (hydrophobic and hydrophilic) into the IVR matrix in a single loading step. The proposed post-loading method can overcome limitations of hot-melt extruded and injection molded IVRs to formulate APIs that are sensitive to high heat and pressure inherent to these processes. Furthermore, this manufacturing process allows the ability to implement geometric complexity within IVRs using computationally aided design (CAD) by eliminating the IVR's solid cross-section and altering drug diffusion distances to fine-tune and control drug diffusion and release kinetics [16, 17].

Our results demonstrated the ability to load two hydrophobic hormonal steroids (ENG and EE) and a hydrophilic ARV (ISL) in a solid 3D-printed silicone poly(urethane) IVR. Our MPT IVR demonstrated long-acting release of ENG/EE/ISL for up to 150 days in vitro. Furthermore, our in vitro data showed no significant ($p > 0.05$) differences in drug release when delivered as an MPT or ARV alone or hormones alone. Additionally, we determined the MPT IVR as chemically and physically stable when stored in 40°C/75% RH for 90 days. Assessing stability under accelerated storage conditions is essential to determining product shelf-life and storage requirements. Post-storage drug release profiles were similar when compared to baseline profiles, with the exception of ISL's burst release which was higher (15.8% burst release) post 90-day storage compared to baseline burst release (4.7% burst release); however, overtime ISL release profile post storage was not significantly different from those recorded at baseline ($p > 0.05$).

The in vivo drug release and PK of the MPT IVR in sheep and ISL IVR in macaques showed sustained drug concentrations in plasma, vaginal fluids, rectal fluids, and vaginal tissue for 14 days in sheep and 28 days in macaques. Plasma ENG/EE levels in sheep that received the CLIP 3D printed MPT IVR (0.2–0.3 mg/kg ENG, 0.05–0.07 mg/kg EE) were 0.3–0.9 ng/mL ENG and 0.01–0.05 ng/mL EE. Hormone levels in sheep with the MPT IVR were slightly lower for ENG compared to average human levels of 1.47 ng/mL and comparable to average human EE levels of 0.0183 ng/mL (0.17 mg/kg ENG, 0.04 mg/kg EE) with NuvaRing after 2 weeks [55]. Future studies include performing a sheep study with NuvaRing to obtain a head-to-head comparison of hormones levels between the two IVRs. Quantification of residual hormones in MPT IVR showed that approximately 37% of ENG

and 24% of EE was released over 14 days in sheep. Since this MPT IVR is intended to be a 90-day ring, future studies will focus on optimizing drug loading and release rate of the hormonal steroids to achieve therapeutic systemic levels that will be sustained over 90 days. Furthermore, ISL plasma levels in sheep (4.03–6.48 mg/kg) were between 0.1–10 ng/mL for the 14-day study duration. ISL IVRs in macaques (4.6–10.3 mg ISL/kg) elicited sustained plasma concentrations (1–10 ng/mL) of ISL for 28 days. Notably, ISL-TP concentrations in macaques were near or above the established oral dosing PK benchmark for protection of 50–100 fmol/10^6 PBMCs. Although we were not able to quantify ISL-TP from sheep PK samples due to the sheep's low ISL phosphorylation capacity, we determined an ISL-TP to ISL in plasma ratio to extrapolate ISL-TP levels from the observed ISL plasma levels in sheep. From this, we estimated that ISL-TP levels were near the established PK benchmark (50–100 fmol/10^6 PBMCs), thus suggesting potential clinical translation to humans.

Additionally, local tolerability and safety of MPT IVR was assessed. In sheep, findings of erythema and petechiae which were seen on colposcopy were consistent with that normally seen in sheep at baseline. There was no evidence of epithelial thinning based on measures from OCT and vaginal biopsies. MPT IVR related findings in sheep were evident as minimal to mild epithelial hyperplasia and parakeratosis with minimal to mild neutrophilic and minimal eosinophilic infiltrates. The epithelial hyperplasia and parakeratosis are likely responses to the estrogenic components in the MPT IVR. A cause for the neutrophils and eosinophils is uncertain, but was not associated with any tissue degeneration or damage, and therefore the finding was not adverse.

Remarkably our studies in sheep and human vaginal mucosa cultures strongly suggested that the MPT IVR surface supported epithelialization and subsequent colonization by commensal and pathobiont bacteria. In particular, sheep IVR had detectable Bacteroides fragilis levels while the human modeling with the BV community showed robust colonization of the mini IVRs (Fig 5 and 6). Despite this colonization no evidence of harm to the sheep mucosa or vaginal epithelial cultures was noted. Molecular data suggested that the MPT and placebo IVRs were efficiently epithelialized within 24 hours of insertion in sheep with increasing levels of sheep cells detected through the 14 study days. Interestingly, the bacterial 16S rDNA copies lagged behind consistent with the conclusion that epithelialization precedes colonization by vaginal microbiota. In similar fashion, GAPDH and 16S rDNA data from the human VEC mucosa culture system supported this conclusion leading to SEM evaluations of the IVR surfaces. Micrographs of IVRs cultured for 48 hours in the VEC system were observed to support attachment of human VEC as well as colonization by bacteria with morphotypes consistent with the VMB present in each culture. These data suggest that IVRs should be tested in multiple contexts to better understand the kinetics of drug release that likely will be impacted by the presence of both VEC and vaginal microbiota. Our release data suggested that the presence of the 'extended mucosal' surface was not a deterrent to successful drug delivery in these models. Our sheep data are limited in that ovine VMB lack the important human Lactobacilli and have very distinct profiles disassociated from the acidic pH found in the human vagina (31, 32) but the data indicating substantial levels of ovine GAPDH and bacterial DNA address the limitation of using immortalized human VEC in our culture model. The complimentary systems provide solid

confirmation that the IVRs are epithelialized and colonized but most importantly were well tolerated and able to effectively deliver drug.

As a final indicator of safety and tolerance of the IVRs, VMB community profiles were molecularly evaluated in sheep and in the human culture model. In sheep, the presence of the MPT IVR led to increases in *E. coli* abundance on both the vaginal wall (swab) and on the IVR itself (wedges and fluid) leading to this organism becoming the dominant bacteria detected by our custom ovine VMB qPCR array (31). In our studies of this breed of sheep treated with vaginal irritants we determined that *E. coli* was associated with reduced inflammation (i.e. reduced inflammatory cytokine levels) and a eubiotic state (32). In the human culture system, testing of the impact of the MPT IVR on three selected VMB communities dominated by *L. crispatus*, a marker of eubiosis, *L. iners*, a marker of transition communities or a BV community (34, 35), did not show significant changes in the profiles suggestive of any toxicity after 48 hours of incubation with either a placebo or mini MPT IVR. The use of both the sheep and human culture model systems allowed greater confidence that the IVRs did not negatively impact the modeled vaginal microbiota however both studies were limited by analysis of DNA rather than viable organisms or functional changes in the bacterial metabolomes. Additional studies would be required well beyond these first safety, tolerability and drug release studies.

The *in vivo* safety of the use of the ISL IVRs was also critically evaluated in macaques to determine if any disturbances to the local vaginal milieu arose due to the extended presence of these rings. The vaginal pH range observed during the presence of the ISL IVR is what is normally seen in pigtailed macaques [47–49]. Concentrations of the mucosal proinflammatory cytokines such as G-CSF, IL-1β, IL-6, IL-8, IL-17, TNF-α, and IFNγ were found to remain stable throughout the study. The presence of the rings for 28 days did not cause any significant changes for all the cytokine and chemokines that were evaluated in this study. The above findings suggest that the ISL IVRs are safe, and the presence of these rings for 28 days does not cause any disturbances to the macaque vaginal microenvironment or result in immune cell reduction.

Furthermore, our results demonstrate the first report of long-acting ISL administered topically with the ability to achieve sustained systemic distribution of ISL-TP in pig-tailed macaques reaching levels near the protective PK benchmark established for oral dosing [27, 31] against SHIV. This is unlike other topically delivered ARVs, which typically result in low systemic concentrations. For example, tenofovir, a hydrophilic ARV that is also intracellularly phosphorylated into its active metabolite, tenofovir-diphosphate, elicited lower drug levels in plasma and higher levels in vaginal tissue and fluids after vaginal administration compared to oral administration [56–58]. This has been observed with several different drug classes when delivered topically via an IVR in macaques [59]. Although ARV plasma levels when administered topically were considerably lower compared to oral administration, the high drug levels in the vaginal tissue and fluids still demonstrated in vitro HIV inhibition in humans [57] and provided protection against SHIV in macaques [59–61]. This trend of low systemic levels when delivered topically is not observed with ISL likely due to ISL-TP's considerably long intracellular half-life (118–171 hours) [62] compared to other ARVs. ISL-TP's long half-life may result in high accumulation in the

systemic circulation potentially explaining the ability to achieve systemic levels similar to oral administration despite being delivered topically. Thus, due to sustained systemic ISL-TP levels observed from our IVRs reaching levels comparable to oral dosing in macaques, we can assume a similar protective benchmark to oral administration or possibly lower because of high ISL concentrations in vaginal and rectal tissues which can act as reservoir contributing to systemic exposure. To confirm this hypothesis, future studies include establishing a PK benchmark for topical administration of ISL with our IVR in macaques.

Additionally, in December 2021, all ISL clinical trials were placed on full or partial hold by the FDA due to a reported decrease in CD4+ cell and lymphocyte counts in peripheral blood after high and repeated doses of ISL [63]. However, clinical trials for once-daily and once-weekly HIV treatment with ISL have recently resumed (September 2022) with a lower ISL dose, but once-monthly PrEP clinical studies have been discontinued [64]. It is unknown if we will observe a similar decrease in immune cell count as the dose and route of administration of ISL differs when administered with our CLIP IVR. We routinely monitor lymphocyte populations in our macaque studies and here we focused on CD4 T cell frequencies in PBMC as a potential safety signal. We chose to further refine the analysis to CD4 subsets. We monitored CD4+CCR5+ population as CCR5 is the primary coreceptor for HIV-1 infection [50], CD4+ naïve and memory populations were included as these immune subsets are required for CD4+ T cell population homeostasis and protection following infection [65]. Moreover, an impaired T cell differentiation has been reported in HIV-1 infected patients receiving antiretroviral therapy during their acute phase of infection (early ART) [66]. A routine monitoring of the systemic CD3, CD8 and CD4 along with the CD4 subtype revealed stable frequencies in PBMC obtained throughout the study. Though we did not monitor for the absolute counts, we did not observe a decrease in the frequency of the CD4 T cells with a sustained release of ISL over 28 days in macaques. The presence of the ISL ring for a greater duration along with the measurement of the T cell absolute counts may be required to determine if a decline like that reported in the clinical trials of ISL will be observed. Thus, for future studies, we plan to perform a dose ranging ISL IVR PK, safety, and efficacy study in non-human primates to establish the safe and efficacious ISL dose required for topical administration. Finally, in future investigations we plan to develop a geometrically complex MPT IVR with the proposed drug regimen to optimize drug loading and accurately fine-tune drug release to achieve target PK and safety in sheep as well as efficacy in non-human primates.

Taken together, our results demonstrate the development of a next-generation 3D-printed MPT IVR that elicits sustained release in vitro and in vivo of three clinically relevant APIs indicated to protect against HIV and unintended pregnancy. Ultimately, this discrete and women-controlled MPT IVR has the potential to elicit high end-user acceptability and adherence and expand preventative options for women and girls around the world, particularly in areas where HIV is most prevalent.

Materials and Methods

Materials

Silicone-urethane based resin (SIL30) was kindly supplied by Carbon Inc. Etonogestrel (ENG) was purchased from Selleckchem (Houston, TX) (Catalog # S4673). Ethinyl estradiol (EE) was purchased from Sigma Aldrich (Saint Louis, MO) (CAS # 57-63-6). Islatravir (ISL) was purchased by Synnovator Inc (CAS #865363-93). Sodium acetate, Solutol-HS 15, and high performance liquid chromatography (HPLC) grade acetonitrile (ACN) with 0.1% trifluoracetic acid, water with 0.1% trifluoracetic acid, isopropyl alcohol, and acetone were purchased from Sigma Aldrich (Saint Louis, MO).

Computational aided design of solid IVRs

Digital light synthesis (DLS) 3D printing was used to fabricate intravaginal rings as previously described [16]. Briefly, a computer aided design (CAD) file was generated in SolidWorks (Dassault Systèmes) and converted to a .STL file, which includes specific IVR design parameters. The IVR template .STL file was imported into Magics (Materialise) and a selected unit cell arrayed into the template using the ‘Scaffold’ feature. Rings were exported as an .STL. Rings were imported into Magics to correct any tessellation errors accumulated during the file transfer processes. Rings were subsequently exported as a .STL for fabrication.

Fabrication of solid IVRs with digital light synthesis (DLS)

Solid IVRs (human-sized, macaque-sized, and mini IVRs) were fabricated in SIL30 with an M1 DLS printer (Carbon, Inc) [16]. SIL30 is a silicone-urethane based resin. IVRs were positioned vertically, and supports were manually added within the Carbon user interface. The two-part SIL30 resin was mixed before dispensing onto the M1 reservoir using a static mixer. Approximately 190 g of SIL30 resin was dispensed onto the M1 reservoir for vertical printing of 16 human-sized solid IVRs (54 mm outer diameter, 7.6 mm cross-sectional diameter) and 130 g for vertical printing of 40 macaque-sized IVRs (25 mm outer diameter, 6.0 mm cross-sectional diameter) per single print fabrication. Mini IVRs (3.0 mm outer diameter, 1.0 mm cross-sectional diameter) were printed similarly for vaginal microbiome studies.

Post-fabrication treatment

After 3D printing fabrication, IVRs were processed with a modified post-fabrication cleaning procedure provided by Carbon [16]. Briefly, IVRs were carefully removed from the build platform and supports were removed using a razor. IVRs were subsequently smoothed where the supports were placed to ensure complete support removal. IVRs were submerged in isopropyl alcohol while shaking for 1 minute and subsequently air dried for 45 minutes. IVRs were then placed in a programmable oven at 120°C for 8 hours to initiate the secondary thermal post cure as previously described [16, 17]. Finally, IVRs were assessed for metrics and dimensions (mass, outer diameter, and cross-sectional diameter) and then stored in 4°C until further use.

High performance liquid chromatography (HPLC)

A reverse-phase HPLC analysis was carried out on an Agilent 1260 HPLC system (Agilent Technologies, Santa Clara, CA, USA) with a Diode Array Detector, and LC pump with autosampler. The stationary phase utilized for the analysis of ENG, EE, and ISL was an Inertsil ODS-3 column (5 μm, 4.6×150 mm) maintained at 40°C. Chromatographic separation was achieved by gradient elution using a mobile phase consisting of 95% water and 5% ACN each with 0.1% trifluoroacetic acid. The flow rate was 1.0 mL/min, and the total run time was 25 minutes for each 25 μL injection. ENG was eluted at 15.2 minutes and measured at 254 nm (LOD and LOQ of 0.244 μg/mL), EE was eluted at 13.8 minutes and measured at 220 nm (LOD of 0.488 μg/mL and LOQ of 0.976 μg/mL), and ISL (LOD of 0.122 μg/mL and LOQ of 0.488 μg/mL) was eluted at 5.9 minutes and measured at 265 nm.

Post-fabrication drug loading and development of loading equations

Post-fabrication absorption of active pharmaceutical ingredients (APIs) results in complete intercalation and homogenous distribution of APIs within the SIL30 IVR matrix as previously described [17]. Briefly, SIL30 parts post-fabrication swell when placed in a drug-containing acetone solution, referred to as loading solution, resulting in drug uptake. Acetone was chosen due to its ability to swell the silicone-based IVR matrix, highly solubilize ENG (89 mg/mL), EE (133 mg/mL), and ISL (23 mg/mL), highly volatile and easily removed during IVR drying step, and is a classified as a Class 3 solvent (low toxicity and low risk to human health) [33]. We utilized a weight-based loading approach to achieve target drug loadings in our IVRs, referred to as loading equations. Loading equations were developed and validated for each API and elicit a linear relationship between drug weight percent ((mass of drug loaded/mass of IVR) × 100) and the concentration of the loading solution. Loading equations were developed by incubating rings in a series of drug concentrated acetone solutions (n=3 IVRs per concentration). Concentrations were chosen to ensure target drug loading would be within the linear range of the output loading equation. Drug concentration in the loading solutions was quantified by HPLC analysis. IVRs were submerged in the loading solution for 24 hours to reach equilibrium swelling, and subsequently air dried overnight followed by drying in an oven under vacuum pressure at 37°C for 48 hours to facilitate acetone removal. To quantify drug loading, dried IVRs were individually submerged in acetone for 48 hours to facilitate drug extraction. Extraction solutions were quantified by HPLC to determine the amount of drug loaded onto each IVR. Loading equations were generated by plotting the concentration of the loading solutions on the x-axis and the weight % ((mass of drug extracted from IVR/initial mass of IVR) × 100) on the y-axis.

Human-sized IVRs for in vitro release studies and sheep studies were loaded in a single step with 14 mg ENG, 3 mg EE, and 300 mg ISL utilizing the APIs respective loading equation. To accomplish this target loading, solid IVRs of known masses were placed in a triple drug loaded acetone solution (0.58 mg/mL ENG, 0.12 mg/mL EE, and 11 mg/mL ISL; 100 mL/IVR) for 24 hours to facilitate drug uptake. IVRs were removed from drug concentrated solution and dried using the aforementioned method. During the drying process, IVRs were massed daily, and drying was considered complete once the mass of IVR reached equilibrium. After drying, n=1 IVR was extracted in 150 mL of acetone for 48 hours to

validate drug loading. Extraction solution was diluted with ACN and quantified on HPLC. Mini IVRs used for vaginal microbiome studies were placed in a similar concentration of ENG/EE/ISL containing acetone solution compared to human-sized solid IVRs for 24 hours to facilitate drug uptake. After drug loading, mini IVRs had approximately 0.25 mg ISL, 0.013 mg ENG, and 0.015 mg EE. Macaque-sized IVRs investigated for in vitro and in in vivo non-human primate studies were loaded with 62 mg ISL. To accomplish this drug loading, macaque-sized IVRs were placed in 9.5 mg/mL ISL in acetone solution for 24 hours to facilitate drug uptake and followed a similar drying described above. To validate drug loading, n=1 IVR was placed in 50 mL of acetone for 48 hours for extraction. Extraction solution was diluted with ACN and quantified with HPLC.

In vitro drug release studies

Drug-loaded human-sized IVRs were placed in 200 mL of simulated vaginal fluid (SVF) at pH 7 (sheep vaginal pH [35]). Drug-loaded macaque-sized IVRs were placed in 100 mL of SVF pH 8 (macaque vaginal pH [44, 49]). All release studies were performed in a USP dissolution apparatus (Vision 8 Elite Dissolution Tester, Hanson) at 60 rpm. The SVF was adapted from Owen and Katz [34] and consisted of 25 mM sodium acetate buffer adjusted to pH 7 (sheep vaginal pH) or 8 (macaque vaginal pH) and 2% Solutol was added to maintain sink conditions. Solutol is a surfactant known to increase the solubility of drugs in release media and ensure sink conditions are achieved throughout the study. Media was completely replaced at day 1, day 4, and weekly to maintain sink conditions. Sink conditions were defined as the drug concentration at or below 1/5 of maximum solubility in SVF with 2% Solutol [67]. Sample aliquots (1 mL) were collected hourly for the first 6 hours, daily for a week, twice weekly for a month, and weekly afterwards. Drug concentration was determined by HPLC analysis with a method developed and validated to analyze all three APIs in a single run. Cumulative drug release was calculated from the HPLC analysis and was normalized to the total mass of drug in the IVR. All experiments were done in triplicate.

Accelerated stability study and post-storage in vitro drug release

Drug-loaded ENG/EE/ISL (MPT) human-sized IVRs (n=4) were placed in sealed plastic bags in a glass chamber at 40°C/75% relative humidity (RH) in a Fisher Scientific Isotemp Incubator (Pittsburgh, PA) [68]. A humidity sensor was placed within the glass chamber to confirm 75% RH. IVR metrics (mass and dimensions) were taken before and after storage. IVRs were removed after 90 days of storage. N=1 IVR was extracted after storage to investigate changes in drug content or drug degradation. A post-storage in vitro release study was conducted to assess differences in drug release after 90 days in accelerated storage conditions compared to baseline (t=0). The post-storage release study was performed in SVF pH 7 and consisted of similar methods for in vitro release as previously described. Release study was performed in triplicate.

Sheep pharmacokinetic and safety with MPT IVR

Sheep studies were approved by the Institutional Animal Care and Use Committee at the University of Texas Medical Branch in Galveston, TX and were performed according to the National Institutes of Health (NIH) Guide for Care and Use of Experimental Animals. Six nonpregnant yearling female Merino sheep were housed indoors with 12:12 light/dark

cycles and chow and water ad libitum. They were fasted overnight prior to each study day and then anesthetized with 5 mg/kg ketamine IM and 0.5–5% isoflurane by facemask and placed supine on a V-tilt table for imaging and sample collections. Imaging with colposcopy as and OCT as previously described [36] was performed. Vaginal biopsies were collected from lateral mid-vagina and processed for hematoxylin and eosin staining. Four sheep were evaluated with imaging and biopsies before and during MPT IVR use. Two sheep were observed with biopsies during a normal estrus cycle over 3 weeks with 3 times weekly evaluations and served as controls for histology comparison.

Histological analysis from sheep vaginal biopsies

Vaginal biopsies were collected and immediately immersed in 10% Neutral Buffered Formalin (Fisher) and allowed to fix for 72 hours prior to routine processing to paraffin, sectioning to 5 μm, and hematoxylin and eosin stained. Samples were evaluated by a board-certified veterinary pathologist. Microscopic findings were graded using a qualitative system of 0–5 (0=no finding; 1=minimal finding; 2=mild finding; 3=moderate finding; 4=marked finding; 5=severe finding).

Analytical methods of sheep and macaque pharmacokinetic samples

All drug concentrations were quantified at the University of North Carolina Center for AIDS Research Clinical Pharmacology and Analytical Chemistry Core, using liquid chromatography–tandem mass spectrometry (LC-MS/MS) methods.

Drug quantification in non-human primate and sheep blood: Plasma was separated from EDTA treated whole blood by centrifugation. Following liquid-liquid extraction (EE and ENG) or protein precipitation (ISL) with isotopically labeled internal standards, plasma analytes were separated using reverse-phase chromatography via a Waters Xterra MS C18 (2.1×50mm, 3.5μm particle size) analytical column for EE and ENG or a Waters Atlantis T3 (2.1×50mm, 3.0μm particle size) for ISL. An AB Sciex API-5000 triple quadruple mass spectrometer was used to detect analytes and internal standards under positive (ENG, ENG-d_7, ISL, $^{13}C^{15}N_3$ ISL) or negative (EE, EE-d_4) ion electrospray conditions. Precision and accuracy of the calibration standards and quality control samples were within 15% for the following dynamic ranges: 0.005–20ng/ml of EE, 0.2–200ng/ml of ENG, and 0.1–100ng/ml of ISL.

PBMCs were isolated from EDTA treated whole blood, counted then lysed in 70:30 methanol:water. Following protein precipitation extraction, the phosphorylated active metabolite (ISL-tp) was separated using anion exchange chromatography via a Thermo Biobasic AX ® (2.1×50mm, 5μm particle size) analytical column. An AB Sciex API-5000 triple quadruple mass spectrometer was used to detect ISL-tp and internal standard ($^{13}C_9$,$^{15}N_3$-dATP) under positive ion electrospray conditions. Precision and accuracy of the calibration standards and quality control samples were within 15% for a dynamic range of 0.05–125ng/ml and final concentrations were reported in fmol/million cells units.

Drug quantification in non-human primate and sheep vaginal and rectal fluids: Mucosal fluid collected onto Merocel sponges was eluted by adding 2mL of

70:30 acetonitrile:water to 15mL Falcon tubes containing a single sponge, vortexing for 1–2 minutes and aliquoting into a 1.5ml microcentrifuge tube. Following protein precipitation and liquid-liquid extraction with isotopically labeled internal standards, EE and ENG were separated using reverse-phase chromatography via a Waters Xterra MS C18 (2.1×50mm, 3.5μm particle size) analytical column. Following protein precipitation extraction with isotopically labeled internal standards, ISL was separated using reverse-phase chromatography via a Waters Atlantis T3 (2.1×50mm, 3.0μm particle size) analytical column for NHP fluids or a Waters Xterra MS C18 (2.1×50mm, 3.5μm particle size) for sheep fluids. An AB Sciex API-5000 triple quadruple mass spectrometer was used to detect analytes and internal standards under positive (ENG, ENG-d_7, ISL, $^{13}C^{15}N_3$-ISL) or negative (EE, EE-d_4) ion electrospray conditions. Precision and accuracy of the calibration standards and quality control samples were within 20% for the following dynamic ranges: 0.05–100ng/ml of EE; 0.2–200ng/ml of ENG; 10–10,000ng/ml of ISL in NHP vaginal fluid; 0.1–500ng/ml in NHP rectal fluid; and 0.01–20000ng/ml in sheep vaginal and rectal fluids.

Drug quantification in non-human primate and sheep tissues: Weighed tissues were transferred into Precellys® hard tissue reinforced metal bead kit tubes (Cayman Chemical Company) containing 1ml of 70:30 acetonitrile:water, homogenized then centrifuged. Following protein precipitation and liquid-liquid extraction with isotopically labeled internal standards, EE and ENG were separated using reverse-phase chromatography via a Waters Xterra MS C18 (2.1×50mm, 3.5μm particle size) analytical column. Following protein precipitation extraction with isotopically labeled internal standards, ISL was separated using reverse-phase chromatography via a Waters Atlantis T3 (2.1×50mm, 3.0μm particle size) analytical column, and ISL-tp was separated using anion exchange chromatography via a Thermo Biobasic AX ® (2.1×50mm, 5μm particle size) analytical column. An AB Sciex API-5000 triple quadruple mass spectrometer was used to detect analytes and internal standards under positive (ENG, ENG-d_7, ISL, $^{13}C^{15}N_3$-ISL, ISL-tp, $^{13}C_9$,$^{15}N_3$-dATP) or negative (EE, EE-d_4) ion electrospray conditions. Precision and accuracy of the calibration standards and quality control samples were within 30% for the following dynamic ranges: 0.025–100ng/ml of EE in sheep tissues; 0.1–500ng/ml of ENG in sheep tissue; 0.025–50ng/ml of ISL and ISL-tp in sheep tissues; 0.1–500ng/ml of ISL in NHP tissues; and 0.1–100ng/ml of ISL-tp in NHP tissues. Final concentrations were normalized to tissue mass and reported in ng/g (ENG, EE, and ISL) or fmol/g (ISL-tp) units.

Vaginal mucosa culture modeling and vaginal microbiome studies

Human vaginal mucosa cultures were created from immortalized vaginal epithelial cells (VEC) in 24 well transwell formats (Greiner Bio-One; Monroe, NC) as previously described (33–36). Matured air-liquid interfaced (ALI) VEC cultures (7 days post air-liquid interface) were colonized with one of three selected VMB communities from de-identified donors including a community dominated by *L. crispatus* (LC), *L. iners* (LI) or a VMB from a donor with clinically-apparent bacterial vaginosis (BV). Mini CLIP IVRs (3 mm O.D.) were applied to the apical surface sterilely and incubated for up to 48 hours before harvesting with sterilized forceps. TEER was performed (34, 35) taking three measurements per sample and reporting that average to represent a biological sample. SEM procedures were described previously (34, 35). DNA was extracted from selected cultures or from IVR wedges using

a Roche MagNAPure 96 system and the associated cell lysis solution (Roche; Indianapolis, IN). Custom qPCR arrays for ovine (31, 32) or human (34, 35) vaginal microbiota have been previously described.

Macaque pharmacokinetic and safety with ISL IVR

The female pigtailed macaques (n=3, age 12–13 years) that were used in this study were housed at the Centers for Disease Control and Prevention in accordance with the standards specified by the Guide for the Care and Use of Laboratory Animals (National Research Council of the Research Academies, 2011). Housing, nutritional, and behavioral policies follow the nonhuman primate guidelines and standard operating procedures of the Comparative Medicine Branch, CDC Atlanta. All sample collection procedures were approved by the CDC Institutional Animal Care and Use Committee (protocol #2955). Animals were sedated for all procedures with an intramuscular injection of 10mg/kg ketamine. ISL IVRs were inserted into the female pigtailed macaques with the aid of a pediatric speculum and forceps on day 0 and remained in place for 28 days. Samples were collected as follows. Vaginal fluid proximal and distal to the cervix, and rectal fluid, were collected on days 0 (prior to ring insertion), 3, 7, 14, 21, 28 and 30 (2 days post ring removal) with merocel spears (BVI, Waltham, MA). The vaginal pH was monitored throughout the study by rolling a Dacron swab with vaginal fluid on a pH colorimetric indicator strip (Millipore, Billerica, MA). Changes in vaginal pH over time were evaluated using Friedman test with Dunn's post-test for multiple comparisons. Vaginal biopsies were obtained on days 7 and 21 with sterile Townsend biopsy instruments with 8mm x 4mm tips. Blood was collected via the saphenous or femoral veins with a 22-gauge needle into cell preparatory tubes (BD Biosciences). Mucosal cytokines and chemokines were monitored by using a Milliplex™ MAP (Millipore, Burlington, Massachusetts) fluorescent multiplexed bead-based assay to determine levels in vaginal fluid obtained during the entire study [48, 69, 70]. The change in mucosal cytokine and chemokine concentrations were monitored by Friedman test of the log transformed values with Dunn's follow up test for multiple comparisons.

Multicolor flow cytometry analysis was performed on PBMC collected during the PK study to monitor for T cell frequencies. The following monoclonal antibodies (clone numbers in parenthesis) CD3− Alexa Fluor 700 (SP34–2), CD20-BV650 (2H7), CD4-V500 (L200), CCR5-PE (3A9), CCR7-PE-Cy7 (3D12), CD45RA-PE-CF594 (5H9), and CD8-V450 (RPA-T8) purchased from BD Biosciences (San Jose, CA) were used. The cells were washed with BD Stain Buffer (FBS Catalog# 554656) and stained with the above surface markers for 30 minutes at 4°C. The mononuclear cells were then fixed with Cytofix and fluorescent data (100,000 events per sample) acquired on LSRII Flow cytometer (BD BioSciences, San Jose, California). It was then analyzed on FlowJo software version 10 (Tree Star, San Carlos, CA). Representative FACS plots (Supplemental Figure S13) of CD4 and CD8 classification based on CD3 and CD20 expression, and expression of CCR5 on CD3+ CD4+ T cells are shown. FACS plot that indicate the expression of CD45RA and CCR7 used to classify the maturational profile of CD3+ CD4+ T cells: CD4+ T_{CM} (central memory CCR7+/CD45RA−) CD4+ naïve (CCR7+/CD45RA+) CD4+T_{EMRA} (terminally differentiated effector memory, CCR7−/CD45RA+) and CD4+T_{EM} (effector

memory, CCR7−/CD45RA− is also included. Changes in frequencies for the different T cell and the CD4 subsets while the IVR was present (days 3,7, 14, 21, and 28 combined as one group) in comparison to prior to ring insertion (day 0) and post IVR removal (day 30) was carried out with Kruskal-Wallis test with Dunn's post-test for multiple comparisons.

Determination of residual drug in MPT IVRs and ISL IVRs from sheep and macaque studies

To determine the residual drug in IVRs that were retrieved after sheep or macaque studies, IVRs were placed in acetone for 48 hours to facilitate extraction. Extraction solution was diluted with ACN and quantified with HPLC.

Determination of ISL phosphorylation capacity in sheep and human PBMCs in vitro

The ISL phosphorylation capacity was determined following a similar protocol as previously described [45]. In brief, sheep and human whole blood in K_2EDTA was shipped from BioIVT (Westbury, NY) at room temperature. PBMCs were isolated by Ficoll separation using lymphocyte separation median (MP Biomedicals) and 50 mL SeptMate centrifuge tubes (STEMCELL Technologies, Cambridge MA). Red blood cells were lysed (eBioscience 1X RBC Lysis Buffer) and PBMCs were stained with Trypan Blue and counted using a hemocytometer. Half a million PBMCs were cultured with 0.5 mL of media (RPMI for human and Iscoves for sheep). All media contained 10% FBS, 1% penicillin/streptomycin, and 10 U/mL of recombinant human IL-2. PBMCs were treated with 5, 50, and 500 ng/mL ISL in triplicate. A stock solution of 1 mg/mL of ISL in DMSO was diluted with the species' media to obtain the desired target concentrations. After ISL treatment, PBMCs were incubated at 37°C for 24 hours. After incubation, the PBMCs were washed was sterile PBS and lysed with 70% methanol in water and stored at −80°C until PK analysis.

Statistical Analysis

Statistical analyses were performed in GraphPad Prism 9 (GraphPad Software, Inc., La Jolla, CA, USA). Two-way ANOVA with Sidak's multiple comparisons tests were performed with respect to timepoint and IVR formulation to assess differences in cumulative in vitro drug release at each timepoint from MPT IVR vs. ISL IVR alone, MPT IVR vs. ENG/EE IVR alone, and MPT IVR before and after storage in accelerated stability conditions. For vaginal microbiota analyses, a student's T test was used to assess differences in the average copies of the sheep GAPDH or bacterial 16S rDNA from vaginal swabs from sheep at baseline (day 0) compared to while the MPT IVR was worn. A multiple t-test with Mann-Whitney corrections was performed to assess differences in TEER values for VEC cultures incubated with no IVR, a placebo IVR, or MPT IVR. For macaque studies, changes in macaque vaginal pH over time were evaluated using Friedman test with Dunn's post-test for multiple comparisons. The change in macaque mucosal cytokine and chemokine concentrations were monitored by Friedman test of the log transformed values with Dunn's follow up test for multiple comparisons. Changes in frequencies for the different T cell and the CD4 subsets while the ISL IVR was present (days 3,7, 14, 21, and 28 combined as one group) in comparison to prior to ring insertion (day 0) and post IVR removal (day 30) was carried out with Kruskal-Wallis test with Dunn's post-test for multiple comparisons. For all statistical tests, a P value of < 0.05 was considered significant (95% confidence level).

Supplementary Material

Refer to Web version on PubMed Central for supplementary material.

Acknowledgments

We would like to thank the UNC Clinical Pharmacology and Analytical Chemistry Core (CPAC), particularly Lauren Tompkins and Brian Van Horne. We would like to thank Jining Zhang of the Topical Prophylaxis Activity, and David Garber, James Mitchell, Frank Deyounks, Shanon Ellis, and Ryan Johnson of the Preclinical Evaluation Team in the CDC Laboratory Branch for their support with the macaque sample collection and processing.

Funding

This work was supported by the National Institute of Allergy and Infectious Diseases (grant number R61AI136002, R01AI162246 and R01AI150358 to S.R.B). The findings and conclusions of this report are those of the author(s) and do not necessarily represent the position of the National Institute of Allergy and Infectious Diseases or Centers for Disease Control and Prevention. This work was also supported by the National Science Foundation Graduate Research Fellowship Program (grant number DGE-1650116 to ICY). The authors would like to thank Professor Joseph M. DeSimone and Carbon, Inc. for supporting this research.

References

[1]. UNAIDS, Global HIV and AIDS Statistics, 2020. https://www.unaids.org/en/resources/fact-sheet. (Accessed January 16, 2023.

[2]. FDA, FDA Approves First Injectable Treatment for HIV Pre-Exposure Prevention, 2021. https://www.fda.gov/news-events/press-announcements/fda-approves-first-injectable-treatment-hiv-pre-exposure-prevention#:~:text=Today%2C%20the%20U.S.%20Food%20and,risk%20of%20sexually%20acquired%20HIV. (Accessed June 22, 2022.

[3]. Trezza C, Ford SL, Spreen W, Pan R, Piscitelli S, Formulation and pharmacology of long-acting cabotegravir, Curr Opin HIV AIDS 10(4) (2015) 239–45. [PubMed: 26049948]

[4]. WHO, WHO continues to support its conditional recommendation for the dapivirine vaginal ring as an additional prevention option for women at substantial risk of HIV, 2021. https://www.who.int/news/item/09-12-2021-who-continues-to-support-its-conditional-recommendation-for-the-dapivirine-vaginal-ring. (Accessed June 22, 2022.

[5]. WHO, WHO recommends the dapivirine vaginal ring as a new choice for HIV prevention for women at substantial risk of HIV infection, 2021. https://www.who.int/news/item/26-01-2021-who-recommends-the-dapivirine-vaginal-ring-as-a-new-choice-for-hiv-prevention-for-women-at-substantial-risk-of-hiv-infection. (Accessed June 22, 2022.

[6]. UNFPA, Nearly half of all pregnancies are unintended—a global crisis, says new UNFPA report, 2022. https://www.unfpa.org/press/nearly-half-all-pregnancies-are-unintended-global-crisis-says-new-unfpa-report. (Accessed June 22, 2022.

[7]. Minnis AM, Krogstad E, Shapley-Quinn MK, Agot K, Ahmed K, Danielle Wagner L, van der Straten A, Team TS, Giving voice to the end-user: input on multipurpose prevention technologies from the perspectives of young women in Kenya and South Africa, Sex Reprod Health Matters 29(1) (2021) 1927477. [PubMed: 34224341]

[8]. van der Straten A, Agot K, Ahmed K, Weinrib R, Browne EN, Manenzhe K, Owino F, Schwartz J, Minnis A, Team TS, The Tablets, Ring, Injections as Options (TRIO) study: what young African women chose and used for future HIV and pregnancy prevention, J Int AIDS Soc 21(3) (2018) e25094. [PubMed: 29600595]

[9]. Weinrib R, Minnis A, Agot K, Ahmed K, Owino F, Manenzhe K, Cheng H, van der Straten A, End-users' product preference across three multipurpose prevention technology delivery forms: Baseline results from young women in Kenya and South Africa, AIDS Behav 22(1) (2018) 133–145. [PubMed: 29052018]

[10]. Young IC, Benhabbour SR, Multipurpose prevention technologies: Oral, parenteral, and vaginal dosage forms for prevention of HIV/STIs and unplanned pregnancy, Polymers (Basel) 13(15) (2021).

[11]. Friend DR, Intravaginal rings: controlled release systems for contraception and prevention of transmission of sexually transmitted infections, Drug Deliv Transl Res 1(3) (2011) 185–93. [PubMed: 25788239]

[12]. Kiser PF, Johnson TJ, Clark JT, State of the art in intravaginal ring technology for topical prophylaxis of HIV infection, AIDS Rev 14(1) (2012) 62–77. [PubMed: 22297505]

[13]. Thurman AR, Clark MR, Hurlburt JA, Doncel GF, Intravaginal rings as delivery systems for microbicides and multipurpose prevention technologies, Int J Womens Health 5 (2013) 695–708. [PubMed: 24174884]

[14]. Malcolm RK, Boyd PJ, McCoy CF, Murphy DJ, Microbicide vaginal rings: Technological challenges and clinical development, Adv Drug Deliv Rev 103 (2016) 33–56. [PubMed: 26829289]

[15]. Murphy DJ, Desjardins D, Boyd P, Dereuddre-Bosquet N, Stimmer L, Caldwell A, Le Grand R, Kelly C, van Roey J, Malcolm RK, Impact of ring size and drug loading on the pharmacokinetics of a combination dapivirine-darunavir vaginal ring in cynomolgus macaques, Int J Pharm 550(1–2) (2018) 300–308. [PubMed: 30153490]

[16]. Janusziewicz R, Mecham SJ, Olson KR, Benhabbour SR, Design and characterization of a novel series of geometrically complex intravaginal rings with digital light synthesis, Advanced Materials Technologies 5(8) (2020) 2000261. [PubMed: 33072856]

[17]. Janusziewicz R, Shrivastava R, Dahl D, Young IC, Bis M, Whitesell A, Benhabbour SR, Fundamental investigation of sustained and controlled therapeutics release from 3D printed medical devices, Materials Today Chemistry 24(100978) (2022) 17.

[18]. Fu J, Yu X, Jin Y, 3D printing of vaginal rings with personalized shapes for controlled release of progesterone, Int J Pharm 539(1–2) (2018) 75–82. [PubMed: 29366944]

[19]. Welsh NR, Malcolm RK, Devlin B, Boyd P, Dapivirine-releasing vaginal rings produced by plastic freeforming additive manufacturing, Int J Pharm 572 (2019) 118725. [PubMed: 31648014]

[20]. Tiboni M, Campana R, Frangipani E, Casettari L, 3D printed clotrimazole intravaginal ring for the treatment of recurrent vaginal candidiasis, Int J Pharm 596 (2021) 120290. [PubMed: 33524521]

[21]. Arany P, Papp I, Zichar M, Regdon G Jr., Beres M, Szaloki M, Kovacs R, Feher P, Ujhelyi Z, Vecsernyes M, Bacskay I, Manufacturing and Examination of Vaginal Drug Delivery System by FDM 3D Printing, Pharmaceutics 13(10) (2021).

[22]. Chen Y, Traore YL, Walker L, Yang S, Ho EA, Fused deposition modeling three-dimensional printing of flexible polyurethane intravaginal rings with controlled tunable release profiles for multiple active drugs, Drug Deliv Transl Res 12(4) (2022) 906–924. [PubMed: 35211869]

[23]. Eder S, Wiltschko L, Koutsamanis I, Afonso Urich JA, Arbeiter F, Roblegg E, Spoerk M, Toward a new generation of vaginal pessaries via 3D-printing: Concomitant mechanical support and drug delivery, Eur J Pharm Biopharm 174 (2022) 77–89. [PubMed: 35390451]

[24]. Tumbleston JR, Shirvanyants D, Ermoshkin N, Janusziewicz R, Johnson AR, Kelly D, Chen K, Pinschmidt R, Rolland JP, Ermoshkin A, Samulski ET, DeSimone JM, Additive manufacturing. Continuous liquid interface production of 3D objects, Science 347(6228) (2015) 1349–52. [PubMed: 25780246]

[25]. Janusziewicz R, Tumbleston JR, Quintanilla AL, Mecham SJ, DeSimone JM, Layerless fabrication with continuous liquid interface production, Proc Natl Acad Sci U S A 113(42) (2016) 11703–11708. [PubMed: 27671641]

[26]. Markowitz M, Sarafianos SG, 4'-Ethynyl-2-fluoro-2'-deoxyadenosine, MK-8591: a novel HIV-1 reverse transcriptase translocation inhibitor, Curr Opin HIV AIDS 13(4) (2018) 294–299. [PubMed: 29697468]

[27]. Markowitz M, Gettie A, St Bernard L, Andrews CD, Mohri H, Horowitz A, Grasperge BF, Blanchard JL, Niu T, Sun L, Fillgrove K, Hazuda DJ, Grobler JA, Once-weekly oral dosing of

MK-8591 protects male rhesus macaques from intrarectal challenge with SHIV109CP3, J Infect Dis 221(9) (2020) 1398–1406. [PubMed: 31175822]

[28]. Barrett SE, Teller RS, Forster SP, Li L, Mackey MA, Skomski D, Yang Z, Fillgrove KL, Doto GJ, Wood SL, Lebron J, Grobler JA, Sanchez RI, Liu Z, Lu B, Niu T, Sun L, Gindy ME, Extended-duration MK-8591-eluting implant as a candidate for HIV treatment and prevention, Antimicrob Agents Chemother 62(10) (2018).

[29]. Matthews RP, Patel M, Barrett SE, Haspeslagh L, Reynders T, Zhang S, Rottey S, Goodey A, Vargo RC, Grobler JA, Stoch SA, Iwamoto M, Safety and pharmacokinetics of islatravir subdermal implant for HIV-1 pre-exposure prophylaxis: a randomized, placebo-controlled phase 1 trial, Nat Med 27(10) (2021) 1712–1717. [PubMed: 34608329]

[30]. Markowitz M, Grobler JA, Islatravir for the treatment and prevention of infection with the human immunodeficiency virus type 1, Curr Opin HIV AIDS 15(1) (2020) 27–32. [PubMed: 31658118]

[31]. Markowitz M, Gettie A, Bernard L, Blanchard J, Grasperge B, Fillgrove K, Xue L, Dube N, Hazuda D, Weekly oral islatravir provides effective PEP against IV challenge with SIVMAC251, Conference on Retroviruses and Opportunistic Infections (CROI), Boston, MA, 2020.

[32]. Urbankova I, Vdoviakova K, Rynkevic R, Sindhwani N, Deprest D, Feola A, Herijgers P, Krofta L, Deprest J, Comparative anatomy of the ovine and female pelvis, Gynecol Obstet Invest 82(6) (2017) 582–591. [PubMed: 28125816]

[33]. FDA, Q3C — Tables and List Guidance for Industry, 2017. https://www.fda.gov/media/71737/download. (Accessed June 22, 2022.

[34]. Owen DH, Katz DF, A vaginal fluid simulant, Contraception 59(2) (1999) 91–5. [PubMed: 10361623]

[35]. Swartz JD, Lachman M, Westveer K, O'Neill T, Geary T, Kott RW, Berardinelli JG, Hatfield PG, Thomson JM, Roberts A, Yeoman CJ, Characterization of the vaginal microbiota of ewes and cows reveals a unique microbiota with low levels of lactobacilli and near-neutral pH, Front Vet Sci 1 (2014) 19. [PubMed: 26664918]

[36]. Vincent KL, Bourne N, Bell BA, Vargas G, Tan A, Cowan D, Stanberry LR, Rosenthal SL, Motamedi M, High resolution imaging of epithelial injury in the sheep cervicovaginal tract: a promising model for testing safety of candidate microbicides, Sex Transm Dis 36(5) (2009) 312–8. [PubMed: 19295469]

[37]. Vincent KL, Vargas G, Wei J, Bourne N, Motamedi M, Monitoring vaginal epithelial thickness changes noninvasively in sheep using optical coherence tomography, Am J Obstet Gynecol 208(4) (2013) 282 e1–7.

[38]. Pyles RB, Miller AL, Maxwell C, Dawson L, Richardson-Harman N, Swartz G, O'Neill C, Walker C, Milligan GN, Madsen T, Motamedi M, Vargas G, Vincent KL, Characterization of the ovine vaginal microbiome and inflammation patterns as an improved testing model of human vaginal irritation, Front Reprod Health 3 (2021) 714829. [PubMed: 36303974]

[39]. Vincent KL, Miller AL, Maxwell C, Richardson-Harman N, O'Neill C, Dawson LN, Madsen T, Walker C, Swartz G, Pyles RB, Development of gram stain scoring system based on pro-inflammatory cytokines in the sheep model for testing toxicity of vaginal products, Front Reprod Health 3 (2021) 714798. [PubMed: 36304006]

[40]. Herbst-Kralovetz MM, Quayle AJ, Ficarra M, Greene S, Rose WA 2nd, Chesson R, Spagnuolo RA, Pyles RB, Quantification and comparison of toll-like receptor expression and responsiveness in primary and immortalized human female lower genital tract epithelia, Am J Reprod Immunol 59(3) (2008) 212–24. [PubMed: 18201283]

[41]. Rose WA 2nd, McGowin CL, Spagnuolo RA, Eaves-Pyles TD, Popov VL, Pyles RB, Commensal bacteria modulate innate immune responses of vaginal epithelial cell multilayer cultures, PLoS One 7(3) (2012) e32728. [PubMed: 22412914]

[42]. Pyles RB, Vincent KL, Baum MM, Elsom B, Miller AL, Maxwell C, Eaves-Pyles TD, Li G, Popov VL, Nusbaum RJ, Ferguson MR, Cultivated vaginal microbiomes alter HIV-1 infection and antiretroviral efficacy in colonized epithelial multilayer cultures, PLoS One 9(3) (2014) e93419. [PubMed: 24676219]

[43]. Herbst-Kralovetz MM, Pyles RB, Ratner AJ, Sycuro LK, Mitchell C, New systems for studying intercellular interactions in bacterial vaginosis, J Infect Dis 214 Suppl 1 (2016) S6–S13. [PubMed: 27449872]

[44]. Patton DL, Sweeney YC, Rabe LK, Hillier SL, The vaginal microflora of pig-tailed macaques and the effects of chlorhexidine and benzalkonium on this ecosystem, Sex Transm Dis 23(6) (1996) 489–93. [PubMed: 8946634]

[45]. Sykes C, Van Horne B, Jones J, Kashuba ADM, Gatto G, Van Der Straten A, Johnson L, Cottrell ML, Intracellular islatravir pharmacology differs between species in an in vitro model: implications for preclinical study design, J Antimicrob Chemother 77(4) (2022) 1000–1004. [PubMed: 35134162]

[46]. Patel M, Zang X, Cao Y, Matthews RP, Plank R, Sklar P, Grobler J, Robertson M, Vargo R, Islatravir PK threshold & dose selection for monthly oral HIV-1 PrEP, Conference on Retroviruses and Opportunistic Infections (CROI), Virtual, 2021.

[47]. Patton DL, Sweeney YC, Cummings PK, Meyn L, Rabe LK, Hillier SL, Safety and efficacy evaluations for vaginal and rectal use of BufferGel in the macaque model, Sex Transm Dis 31(5) (2004) 290–6. [PubMed: 15107631]

[48]. Srinivasan P, Zhang J, Martin A, Kelley K, McNicholl JM, Buckheit RW Jr., Smith JM, Ham AS, Safety and pharmacokinetics of quick-dissolving polymeric vaginal films delivering the antiretroviral IQP-0528 for preexposure prophylaxis, Antimicrob Agents Chemother 60(7) (2016) 4140–50. [PubMed: 27139475]

[49]. Pereira LE, Clark MR, Friend DR, Garber DA, McNicholl JM, Hendry RM, Doncel GF, Smith JM, Pharmacokinetic and safety analyses of tenofovir and tenofovir-emtricitabine vaginal tablets in pigtailed macaques, Antimicrob Agents Chemother 58(5) (2014) 2665–74. [PubMed: 24566178]

[50]. Jasinska AJ, Pandrea I, Apetrei C, CCR5 as a coreceptor for human immunodeficiency virus and simian immunodeficiency viruses: A prototypic love-hate affair, Front Immunol 13 (2022) 835994. [PubMed: 35154162]

[51]. Merck, Merck Announces Clinical Holds on Studies Evaluating Islatravir for the Treatment and Prevention of HIV-1 Infection, 2021. https://www.merck.com/news/merck-announces-clinical-holds-on-studies-evaluating-islatravir-for-the-treatment-and-prevention-of-hiv-1-infection/. (Accessed June 20 2022).

[52]. Merck, Merck to Initiate New Phase 3 Clinical Program with Lower Dose of Daily Oral Islatravir in Combination with Doravirine for Treatment of People with HIV-1 Infection, 2022. https://www.merck.com/news/merck-to-initiate-new-phase-3-clinical-program-with-lower-dose-of-daily-oral-islatravir-in-combination-with-doravirine-for-treatment-of-people-with-hiv-1-infection/. (Accessed September 27 2022).

[53]. Hendrix C, Hillier S, Bekker LG, Badal-Faesen S, Riddler S, Fuchs E, MacDonald P, Edick S, Plank R, Chavez-Eng C, Evans B, Zang X, Vargo R, Robertson M, Patel M, Islatravir distribution in mucosal tissue, PBMC, and plasma after monthly oral dosing, Conference on Retroviruses and Opportunistic Injections, Virtual, 2022.

[54]. Simiele M, D'Avolio A, Baietto L, Siccardi M, Sciandra M, Agati S, Cusato J, Bonora S, Di Perri G, Evaluation of the mean corpuscular volume of peripheral blood mononuclear cells of HIV patients by a coulter counter to determine intracellular drug concentrations, Antimicrob Agents Chemother 55(6) (2011) 2976–8. [PubMed: 21402849]

[55]. FDA, NuvaRing® (etonogestrel/ethinyl estradiol) vaginal ring, 2013. https://www.accessdata.fda.gov/drugsatfda_docs/nda/2013/021187Orig1s021.pdf. (Accessed June 20, 2022.

[56]. Karim SS, Kashuba AD, Werner L, Karim QA, Drug concentrations after topical and oral antiretroviral pre-exposure prophylaxis: implications for HIV prevention in women, Lancet 378(9787) (2011) 279–81. [PubMed: 21763939]

[57]. Ouattara LA, Thurman AR, Jacot TA, Cottrell M, Sykes C, Blake K, Fang X, Ju S, Vann NC, Schwartz J, Doncel GF, Genital mucosal drug concentrations and anti-HIV activity in

tenofovir-based PrEP products: Intravaginal ring vs. oral administration, J Acquir Immune Defic Syndr 89(1) (2022) 87–97. [PubMed: 34878438]

[58]. Hendrix CW, Chen BA, Guddera V, Hoesley C, Justman J, Nakabiito C, Salata R, Soto-Torres L, Patterson K, Minnis AM, Gandham S, Gomez K, Richardson BA, Bumpus NN, MTN-001: randomized pharmacokinetic cross-over study comparing tenofovir vaginal gel and oral tablets in vaginal tissue and other compartments, PLoS One 8(1) (2013) e55013. [PubMed: 23383037]

[59]. Smith JM, Srinivasan P, Teller RS, Lo Y, Dinh CT, Kiser PF, Herold BC, Tenofovir disoproxil fumarate intravaginal ring protects high-dose depot medroxyprogesterone acetate-treated macaques from multiple SHIV exposures, J Acquir Immune Defic Syndr 68(1) (2015) 1–5. [PubMed: 25321184]

[60]. Smith JM, Rastogi R, Teller RS, Srinivasan P, Mesquita PM, Nagaraja U, McNicholl JM, Hendry RM, Dinh CT, Martin A, Herold BC, Kiser PF, Intravaginal ring eluting tenofovir disoproxil fumarate completely protects macaques from multiple vaginal simian-HIV challenges, Proc Natl Acad Sci U S A 110(40) (2013) 16145–50. [PubMed: 24043812]

[61]. Srinivasan P, Zhang J, Dinh CT, Teller RS, McNicholl JM, Kiser PF, Herold BC, Smith JM, Repeated administration of high-dose depot medroxyprogesterone acetate does not alter SHIVSF162p3 viral kinetics and tenofovir pharmacokinetics when delivered via intravaginal rings, J Med Primatol 46(4) (2017) 129–136. [PubMed: 28748662]

[62]. Matthews RP, Ankrom W, Friedman E, Jackson Rudd D, Liu Y, Mogg R, Panebianco D, De Lepeleire I, Petkova M, Grobler JA, Stoch SA, Iwamoto M, Safety, tolerability, and pharmacokinetics of single- and multiple-dose administration of islatravir (MK-8591) in adults without HIV, Clin Transl Sci 14(5) (2021) 1935–1944. [PubMed: 34463432]

[63]. Merck, Merck announces clinical holds on studies evaluating islatravir for the treatment and prevention of HIV-1 infection, 2021. https://www.merck.com/news/merck-announces-clinical-holds-on-studies-evaluating-islatravir-for-the-treatment-and-prevention-of-hiv-1-infection/. (Accessed June 20, 2022.

[64]. Merck, Merck to initiate new phase 3 clinical program with lower dose of daily oral islatravir in combination with doravirine for treatment of people with HIV-1 infection, 2022. https://www.merck.com/news/merck-to-initiate-new-phase-3-clinical-program-with-lower-dose-of-daily-oral-islatravir-in-combination-with-doravirine-for-treatment-of-people-with-hiv-1-infection/. (Accessed September 27, 2022.

[65]. Gray JI, Westerhof LM, MacLeod MKL, The roles of resident, central and effector memory CD4 T-cells in protective immunity following infection or vaccination, Immunology (2018).

[66]. Petkov S, Chiodi F, Impaired CD4+ T cell differentiation in HIV-1 infected patients receiving early anti-retroviral therapy, Genomics 114(3) (2022) 110367. [PubMed: 35429609]

[67]. Liu P, De Wulf O, Laru J, Heikkila T, van Veen B, Kiesvaara J, Hirvonen J, Peltonen L, Laaksonen T, Dissolution studies of poorly soluble drug nanosuspensions in non-sink conditions, AAPS PharmSciTech 14(2) (2013) 748–56. [PubMed: 23615772]

[68]. Greenspan L, Humidity fixed points of binary saturated aqueous solutions, Journal of Research of the National Bureau of Standards- A. Physics and Chemistry 81A(1) (1997) 89–96.

[69]. Johnson TJ, Clark MR, Albright TH, Nebeker JS, Tuitupou AL, Clark JT, Fabian J, McCabe RT, Chandra N, Doncel GF, Friend DR, Kiser PF, A 90-day tenofovir reservoir intravaginal ring for mucosal HIV prophylaxis, Antimicrob Agents Chemother 56(12) (2012) 6272–83. [PubMed: 23006751]

[70]. Srinivasan P, Dinh C, Zhang J, Pau CP, McNicholl JM, Lo Y, Herold BC, Teller R, Kiser P, Smith JM, Pharmacokinetic evaluation of tenofovir disoproxil fumarate released from an intravaginal ring in pigtailed macaques after 6 months of continuous use, J Med Primatol 43(5) (2014) 364–9. [PubMed: 25379594]

Highlights

- ENG/EE/ISL were loaded into the IVR in a single step using a controlled solvent-mediated loading process
- ENG/EE/ISL IVRs exhibited sustained release for 150 days in vitro and 14 days in sheep
- ISL IVRs exhibited sustained release in macaques for 28 days above the PK benchmark
- IVRs showed no signs of toxicity in sheep, modeled human vaginal mucosa, and macaques

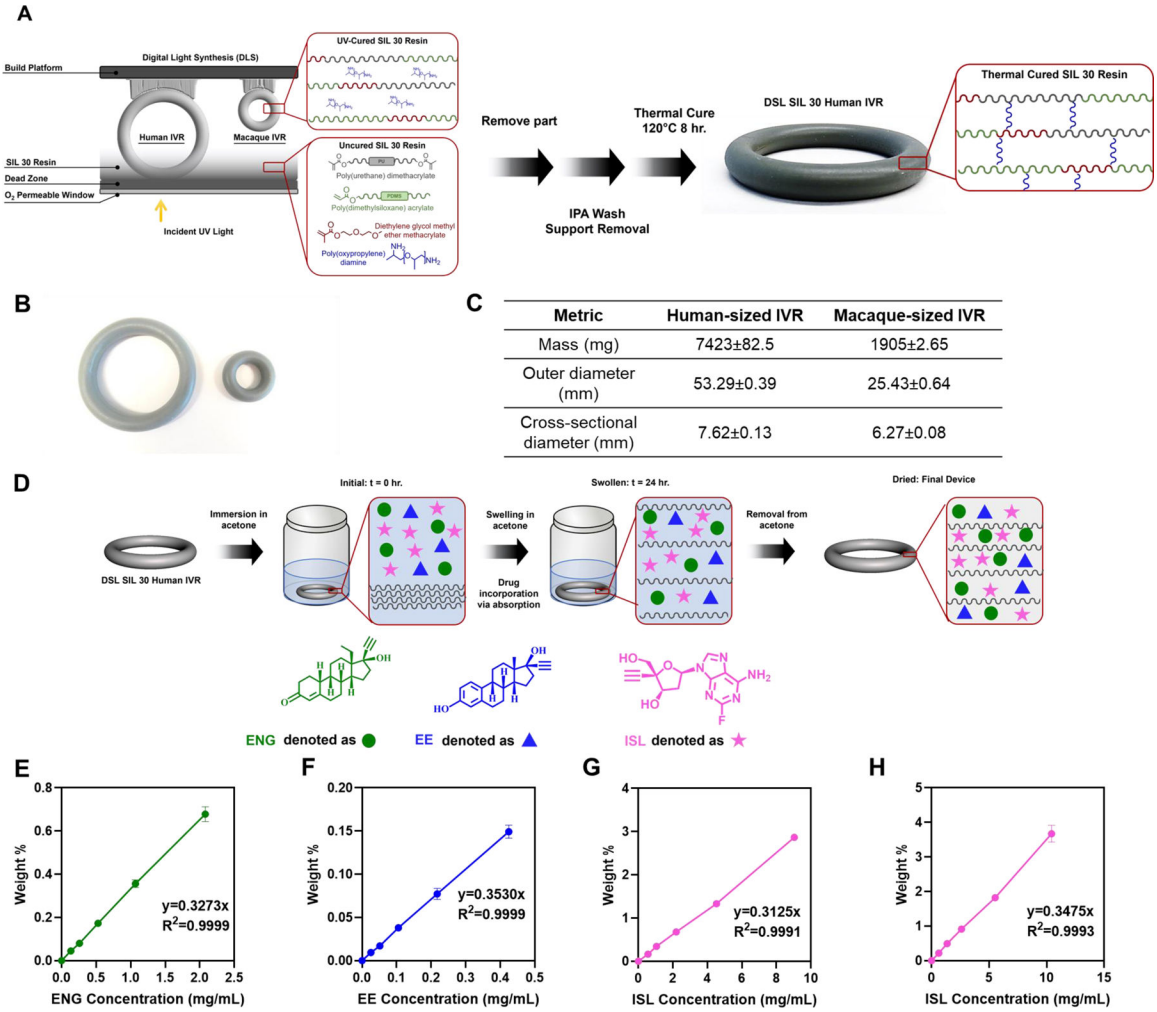

Figure 1. CLIP IVR fabrication, drug incorporation, and loading equations.

(A) Schematic of human-sized and macaque-sized IVR fabrication with CLIP 3D-printing. Complete IVR fabrication with CLIP includes a UV and thermal cure for complete matrix formation driven by free-radical photo-polymerization mechanisms. Dual SIL30 resin is first exposed to UV light during the 3D printing process followed by an IPA (isopropyl alcohol) wash to remove excess resin. A secondary thermal cure completes matrix formation to achieve the final silicone IVR matrix. Matrix properties remain the same with human or macaque sized IVRs. (B) Human-sized solid CLIP (SIL30) IVR used for sheep studies (left) and macaque-sized CLIP (SIL30) IVR (right). (C) Summary table of average metrics and dimensions of human- and macaque-sized IVRs. (D) Schematic of IVR drug incorporation process driven by absorption mechanisms. The SIL30 IVR is placed an ENG/EE/ISL acetone solution for 24 hours to promote IVR matrix swelling resulting in drug uptake. After drug loading, IVRs are removed from the drug-loaded solution and IVRs return to their initial state with no changes in the matrix from swelling or drug absorption processes. Human-sized IVR loading equations of (E) ENG, (F) EE, and (G) ISL. (H) ISL loading equation with macaque-sized IVRs.

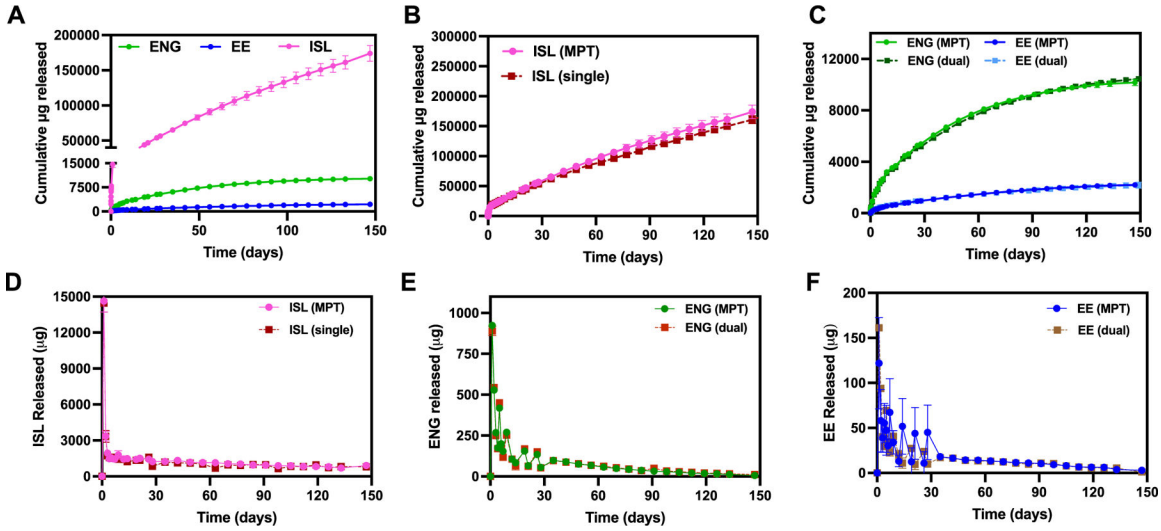

Figure 2. In vitro release of MPT IVR (ENG/EE/ISL IVR), ISL IVR, and ENG/EE IVR.

(A) Cumulative µg release of ISL/ENG/EE from MPT IVR. (B) Cumulative µg release of ISL (single) when formulated alone in IVR compared to release as an MPT. (C) Cumulative µg release of ENG/EE (dual) when formulated alone in IVR compared to release as an MPT. (D) Daily release (µg) of ISL as an MPT and when formulated alone. (E) Daily release (µg) of ENG as an MPT and when formulated without ISL. (F) Daily release (µg) of EE as an MPT and when formulated without ISL. All experiments were performed in triplicate in SVF pH 7 (average ± standard deviation).

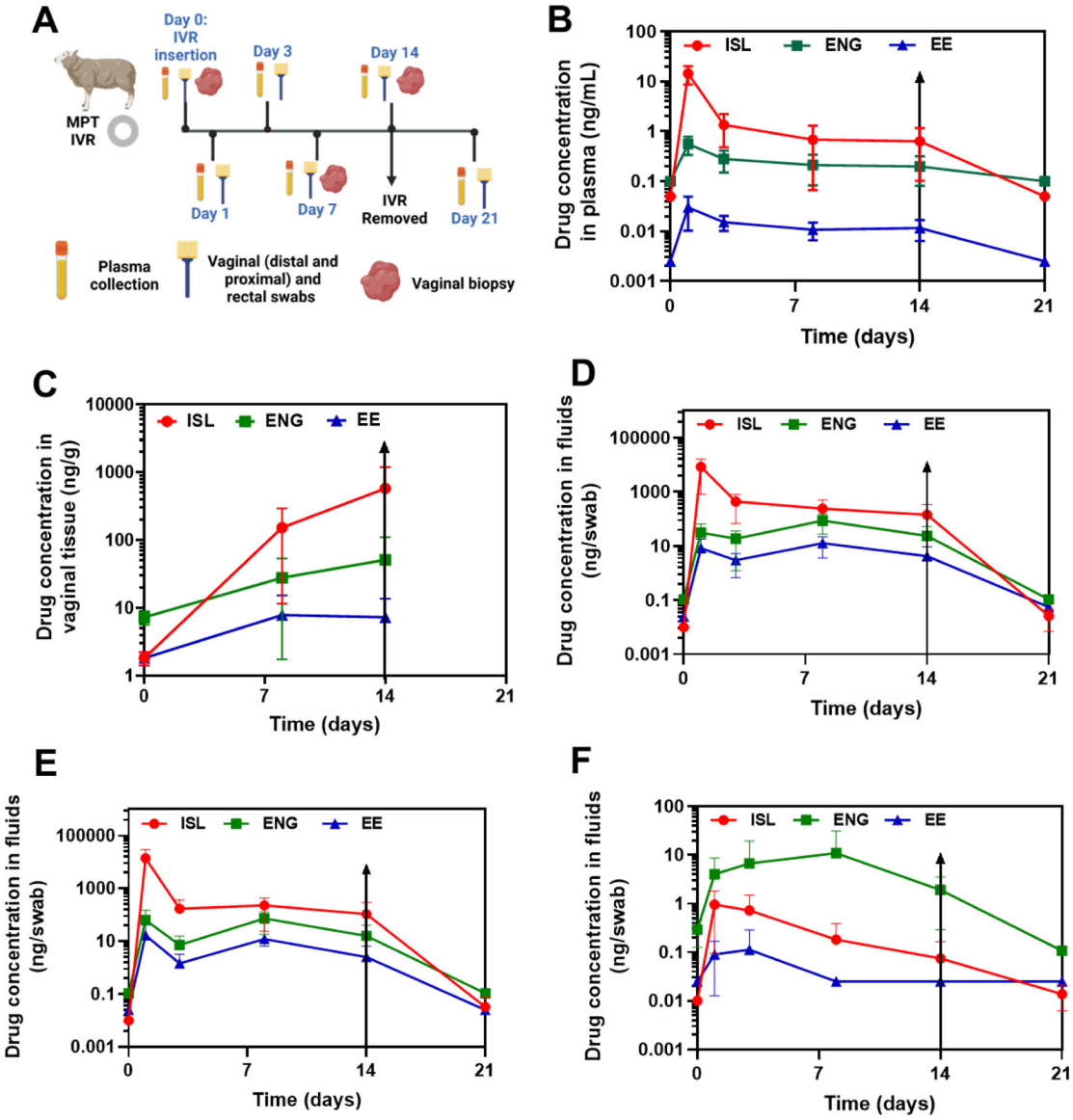

Figure 3. Sheep pharmacokinetics of MPT IVR.

(A) Sheep PK study design (Figure created with BioRender.com). Drug concentration of ENG/EE/ISL in (B) plasma (ng/mL), (C) vaginal tissue (ng/g), (D) proximal vaginal fluids (ng/swab), (E) distal vaginal fluids (ng/swab), and (F) rectal fluids (ng/swab). Black arrows represent IVR removal. Error bars represent the standard deviation of the mean of n=4 female sheep. Each sheep received 4.03–6.48 mg/kg ISL, 0.2–0.3 mg/kg ENG, and 0.05–0.07 mg/kg EE. Lower limit of quantification (LLOQ) values for the APIs were as followed: ISL LLOQ of 0.1 ng/mL in plasma, 4.24 ng/g in tissue, and 0.0215 ng/swab in fluids; ENG LLOQ of 0.2 ng/mL in plasma, 17 ng/g in tissue, 0.215 ng/swab in fluids; EE LLOQ of 0.005 ng/mL in plasma, 4.2 ng/swab in tissue, and 0.05 ng/swab in fluids. Samples that were below the limit of quantification were represented as LLOQ/2. Individual replicates for ENG, EE, and ISL in MPT IVR are shown in Figure S3, S4, and S5, respectively and median (range) values are shown in Table S1–3.

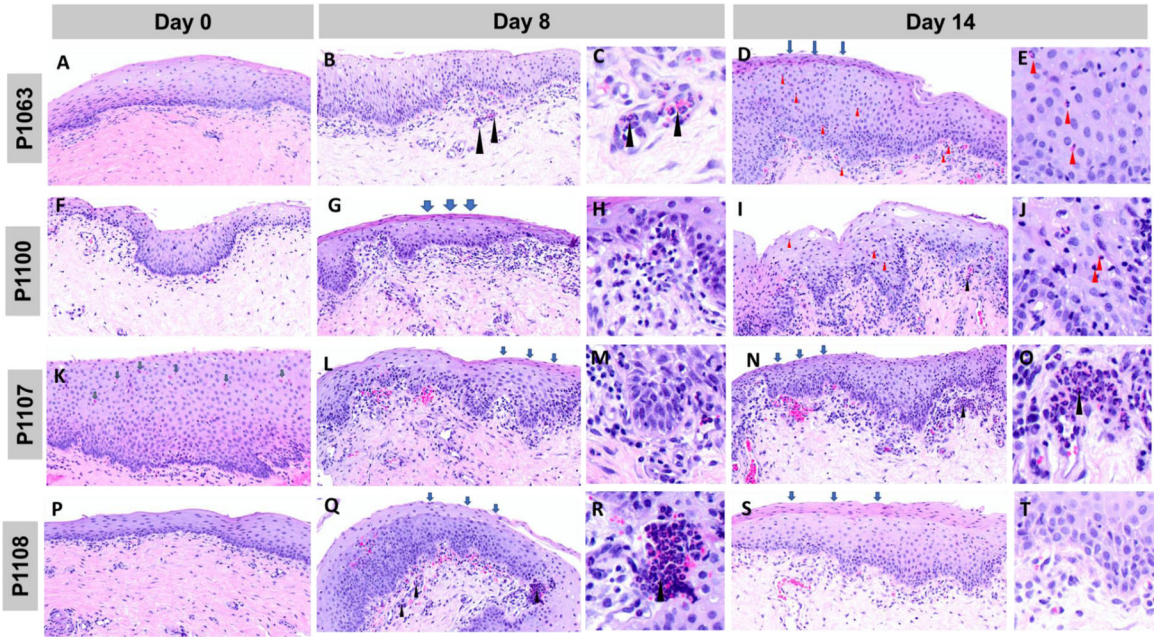

Figure 4. Histology and safety of sheep vaginal tissue biopsies after IVR administration.

(A-E) Sheep ID P1063 histological images of vaginal tissue at (A) day 0 (before IVR administration), (B) day 8 (post-IVR administration), (C) zoomed-in image of (B) to emphasize neutrophils, (D) day 14 (post-IVR administration), (E) zoomed-in image of (D) to emphasize eosinophils. (F-J) Sheep ID P1100 histological images of vaginal tissue at (F) day 0 (before IVR administration), (G) day 8 (post-IVR administration), (H) zoomed-in image of (G), (I) day 14 (post-IVR administration), (J) zoomed-in image of (I) to emphasize eosinophils. (K-N) Sheep ID P1107 histological images of vaginal tissue at (K) day 0 (before IVR administration), (L) day 8 (post-IVR administration), (M) zoomed-in image of (L) (N) day 14 (post-IVR administration), (O) zoomed-in image of (N) to emphasize neutrophils. (P-T) Sheep ID P1108 histological images of vaginal tissue at (P) day 0 (before IVR administration), (Q) day 8 (post-IVR administration), (R) zoomed-in image of (Q) to emphasize neutrophils (S) day 14 (post-IVR administration), (T) zoomed-in image of (S). Blue arrows indicate parakeratosis, black arrows represent neutrophils, and red arrows represent eosinophils. Semi-quantitative scoring is shown in Figure S6.

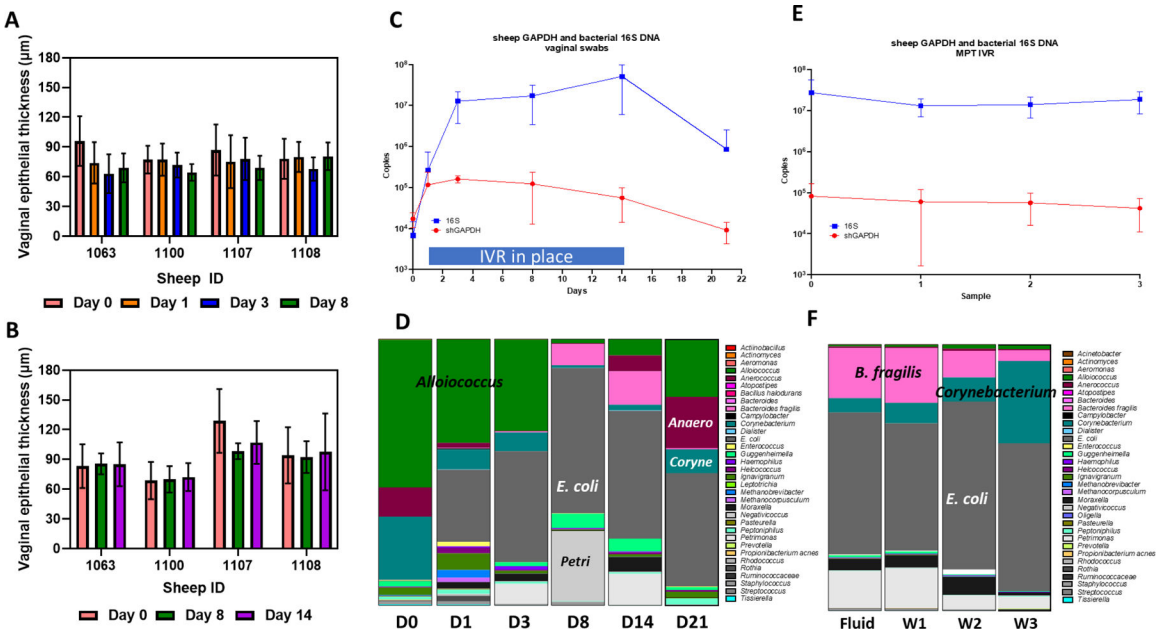

Figure 5. Impact of MPT IVRs on sheep vaginal mucosa and vaginal microbiota

(**A**) Vaginal epithelial thickness (µm) measured by optical coherence tomography (OCT) over the first 8 days of treatment with the MPT IVR did not show thinning (error bars indicate standard deviation). (**B**) Vaginal epithelial thickness (µm) measured on H&E from a single biopsy from each sheep did not show epithelial thinning during the course of the treatment with the MPT IVR (error bars indicate standard deviation) and were similar to naturally cycling control sheep (N=2, no treatment IVR). (**C**) The average copies of the sheep GAPDH (red line) or bacterial 16S rDNA (blue line) from vaginal swabs from the 4 animals were quantified by PCR (qPCR) are shown (± standard deviation) at baseline (day 0) and then 24 hours after IVR placement through day 14 and then again on day 21, 7 days after the rings were removed. (**D**) Proportional bar charts, generated using a custom qPCR array, showing the average vaginal bacterial community profile in vaginal swabs from the 4 sheep are shown illustrating the average change with increasing levels of *E. coli* and decreasing proportions of *Alloiococcus* while the IVR was present. (**E**) The 4 removed MPT IVRs were processed sterilely allowing analysis of both sheep GAPDH (red line) and bacterial 16S (blue line) copies using the same qPCR analyses. The fluid carried by the ring (sample 0) was compared to the material adhered to each of 3 equidistant wedges (samples 1–3) from each of the 4 MPT IVRs. (**F**) Average bacterial profiles, determined by the custom qPCR array), are shown proportionally for the ring fluid and the three wedges indicating a dominance of *E. coli* an organism associated with ovine vaginal eubiosis (31, 32).

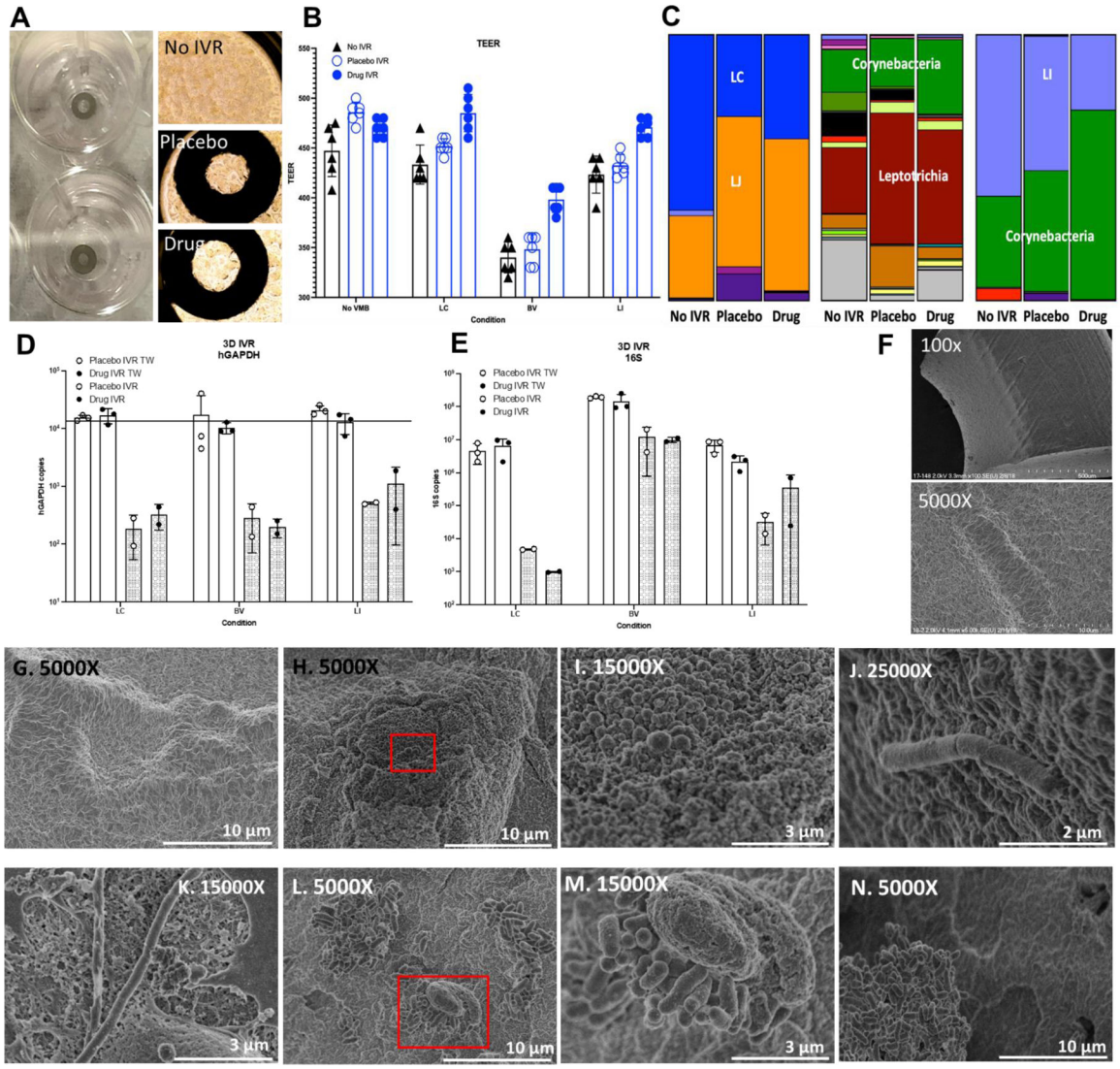

Figure 6. Human vaginal microbiota studies with mini MPT IVRs

(**A**) The left panel shows matured air-liquid interfaced (ALI) VEC cultures in 24well format transwells cultured with mini MPT IVRs. For this initial study, triplicate cultures were incubated with or without the indicated IVRs for 48h before phase imaging (4X magnification) showing no obvious impact on the health or integrity of the multilayers (right panels). (**B**) TEER values for 6 replicates of VEC cultures incubated with no IVR (black), a placebo IVR (open blue) or MPT (drugged) IVR (filled blue) for 48h were established. Parallel ALI VEC cultures were established with one of three selected vaginal microbiome (VMB) communities dominated by *Lactobacillus crispatus* (LC), bacterial vaginosis (BV) organisms or *L. iners* (LI) by colonization for 24 hour prior to placement of the IVR. (**C**) Proportional bar charts showing the relative abundance of bacteria in the three tested VMB communities were established by qPCR array analysis. Parallel cultures (n=3) without MPT IVRs were compared to placebo or MPT (drugged) IVRs. (**D**) Average human GAPDH copies were established for ALI VEC cultures that had no VMB or IVR (horizontal line) and compared to placebo (open symbol) or MPT (drugged) IVRs (filled symbol) incubated

in cultures with each of the 3 selected VMBs (open bars show average ± SDEV). Similarly, average human GAPDH levels on IVRs (n= 2) were established for each condition (grey bars). No significant differences were observed. (**E**) Bacterial 16S rDNA copies were similarly compared for both ALI VEC cultures (open bars) and IVRs (grey bars) with no significant differences other than the expected increased levels associated with the BV community. (**F**) Scanning electron micrographs (SEM) imaging completed at 100X (dry unused IVR; top) and 5000X (medium-soaked IVR; bottom) showed the surface of a mini MPT IVR. (**G-N**) SEM images of IVR surfaces after 48h in VEC culture. (**G**) IVR soaked in culture medium only; (**H & I**) A field of epithelia at low and high magnification [(**I**) is the identified region in (**H**)] of the apical surface of an IVR cultured in VEC without microbiota; (**J**) Apical surface of an IVR cultured in VEC colonized with the LC-dominated community showing a bacillus morphotype; (**K**) IVR apical surface from an ALI VEC culture colonized with the LI-dominated community highlighting a representative bacillus morphotype; (**L-N**). Apical surfaces of IVRs from a BV-colonized VEC culture [(**L**) is the identified region in (**M**)] illustrating multiple morphotypes and higher bacterial density consistent with the BV community profile. Magnifications and scale bars for each image are as indicated.

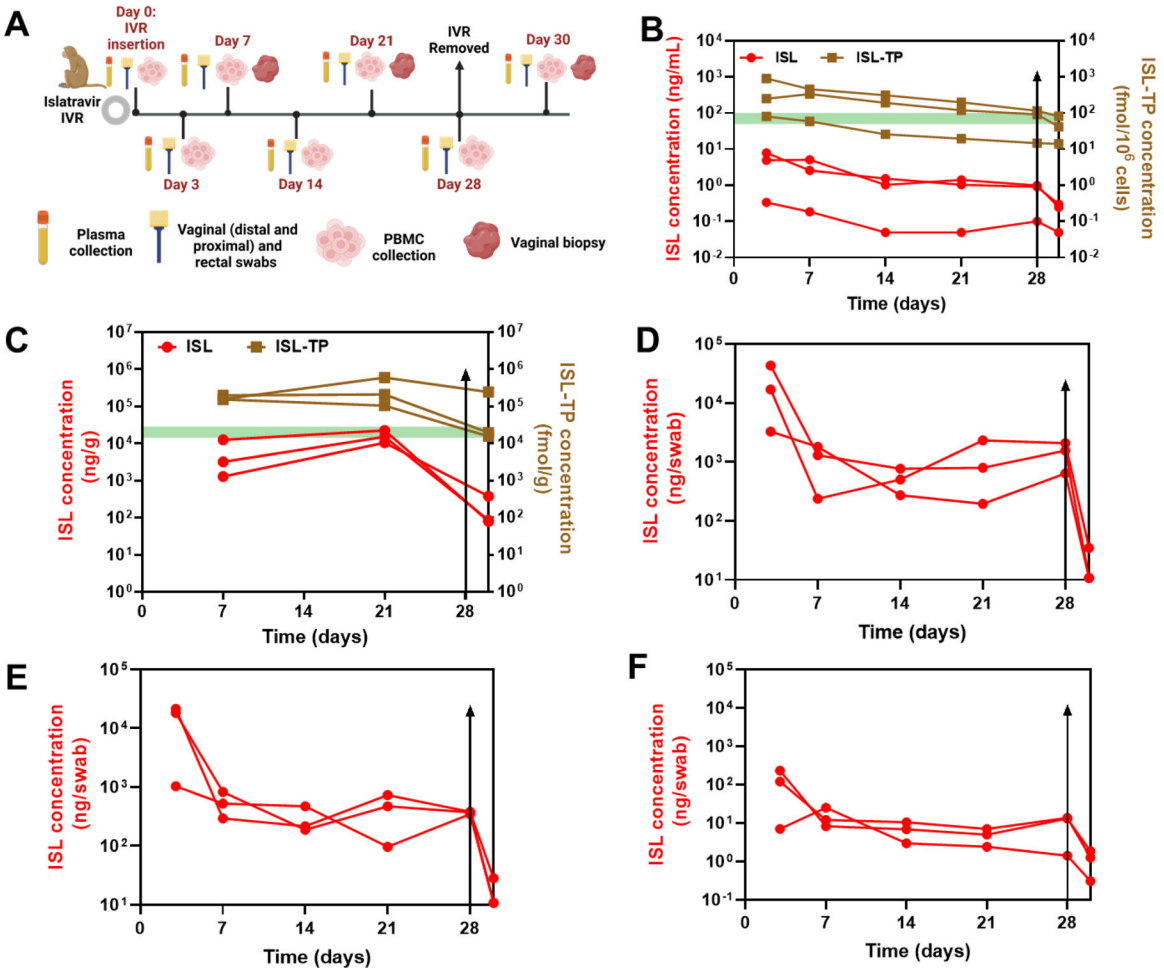

Figure 7. Macaque pharmacokinetics of ISL IVR.

(A) Macaque PK study design (Figure made in BioRender.com). Average drug concentrations of ISL and ISL-triphosphate (TP) in (B) plasma (ng/mL), (C) vaginal tissue (ng/g), (D) proximal vaginal fluids (ng/swab), (E) distal vaginal fluids (ng/swab), and (F) rectal fluids (ng/swab) from n=3 female macaques (average ± standard deviation). Red curves represent ISL levels and brown curves represent ISL-TP levels for n=3 macaques. Black arrow represents IVR removal. The green bar in (B) denotes 50–100 fmol/10^6 PBMCs, which is the established ISL-TP PK benchmark for oral administration [46]. The green bar in (C) denotes PK benchmark of 50–100 fmol/10^6 PBMCs converted to fmol/g of tissue based on a conversion factor of 284,355 cells/mg of tissue. Each macaque received 4.6–10.3 mg/kg ISL. Lower limit of quantification (LLOQ) for ISL and ILS-TP in plasma was 0.10 ng/mL and 9.38 fmol/10^6 PBMCs, respectively. LLOQ for ISL and ISL-TP in vaginal tissue was 26.2 ng/g and 258769 fmol/g, respectively. LLOQ for ISL in fluids was 21.5 ng/swab. Samples that were below the limit of quantification were represented as LLOQ/2. Median (range) values for plasma, vaginal tissue, and fluids are shown in Table S4–6, respectively.

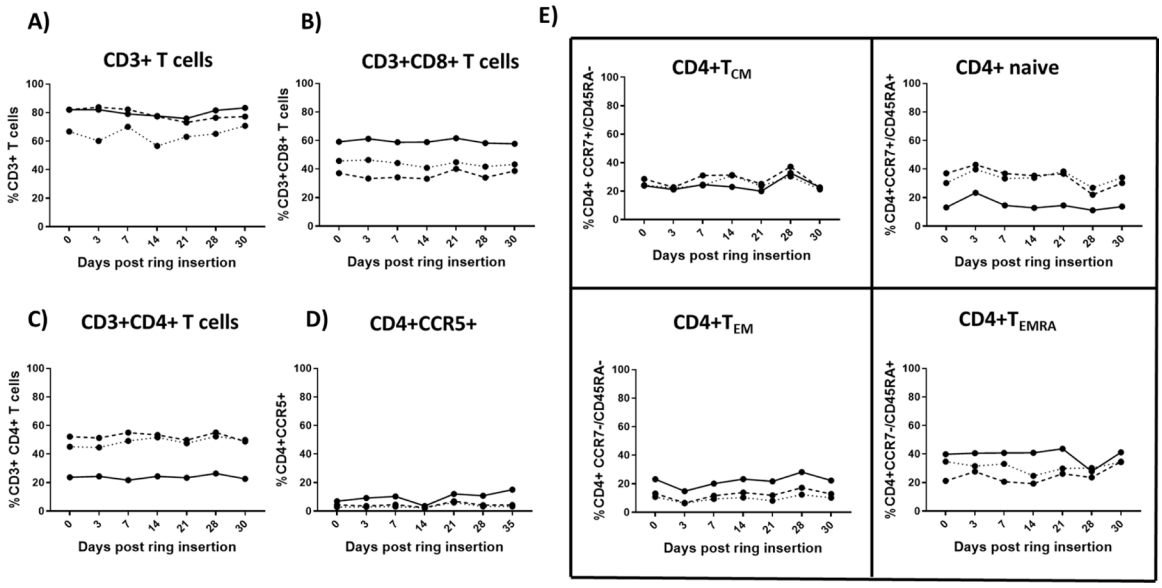

Figure 8. T cell frequencies in PBMC in macaques that received ISL IVRs.

T cell frequencies (A) CD3+ (B) CD3+CD8+ (C) CD3+CD4+ and (D) CD4+CCR5+ were determined from the PBMC collected throughout the study from all three animals. (E) The expression of CD45RA and CCR7 was used to classify the maturational profile of CD3+ CD4+ T cells: CD4+ T_{CM} (central memory CCR7+/CD45RA−) CD4+ naïve (CCR7+/CD45RA+) CD4+T_{EMRA} (terminally differentiated effector memory, CCR7−/CD45RA+) and CD4+T_{EM} (effector memory, CCR7−/CD45RA−). Samples obtained prior to ring insertion (Day 0) and post removal (Day 30) were included along with PBMC obtained while the IVR was present (days 3–28). Each animal is represented independently (PRM2 dashed line, PFN2 dotted line, B0315 solid line).

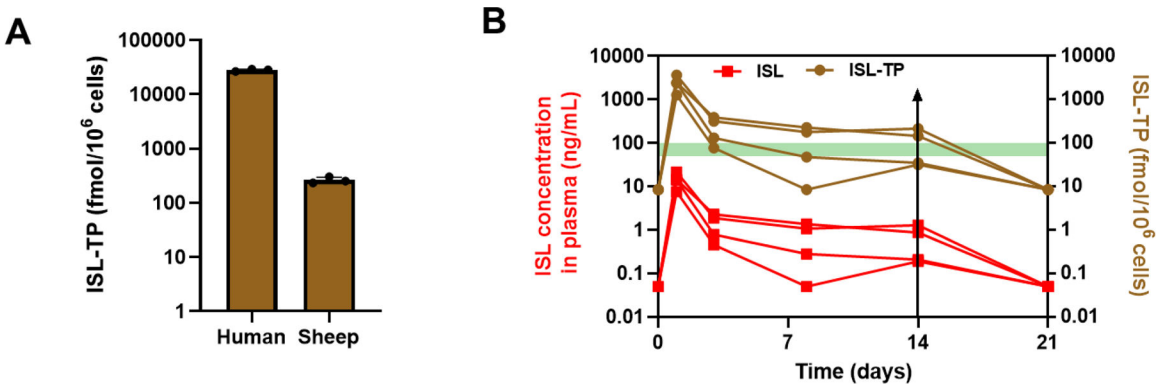

Figure 9. Extrapolation of ISL-TP levels in sheep.

(A) ISL phosphorylation capacity in human and sheep PBMCs after 500 ng/mL ISL dosing (n=3/species). (B) Estimation of ISL-TP levels in sheep. Red lines indicate observed ISL levels in plasma from sheep PK study (n=4). Brown lines represent estimated ISL-TP levels extrapolated using ISL-TP to ISL plasma ratio. Ratio was calculated using ISL IVR macaque PK data by converting ISL-TP and ISL plasma levels to nM. The conversion of nM from fmol/10^6 PBMCs was made using the assumption that one PBMC has an approximate volume of 282 fL [54]. Green bar represents established ISL-TP PK oral benchmark (50–100 fmol/10^6 PBMCs) [46]. Black arrow represents IVR removal.